

Spectral Energy Distributions of Young Stars in IC 348: The Role of Disks in Angular Momentum Evolution of Young, Low-Mass Stars

Thompson S. Le Blanc^{1,2}, Kevin R. Covey^{3,4}, Keivan G. Stassun^{1,5}

ABSTRACT

Theoretical work suggests that a young star’s angular momentum content and rotation rate may be strongly influenced by magnetic interactions with its circumstellar disk. A generic prediction of these ‘disk-locking’ theories is that a disk-locked star will be forced to co-rotate with the Keplerian angular velocity of the inner edge of the disk; that is, the disk’s inner truncation radius should equal its co-rotation radius. These theories have also been interpreted to suggest a gross correlation between young stars’ rotation periods and the structural properties of their circumstellar disks, such that slowly rotating stars possess close-in disks that enforce the star’s slow rotation, whereas rapidly rotating stars possess anemic or evacuated inner disks that are unable to brake the stars and instead the stars spin up as they contract. To test these expectations, we model the spectral energy distributions of 33 young stars in IC 348 with known rotation periods and infrared excesses indicating the presence of circumstellar disks. For each star, we match the observed spectral energy distribution, typically sampling 0.6–8.0 μm , to a grid of 200,000 pre-computed star+disk radiative transfer models, from which we infer the disk’s inner-truncation radius. We then compare this truncation radius to the disk’s co-rotation radius, calculated from the star’s measured rotation period. We do not find obvious differences in the disk truncation radii of slow rotators vs. rapid rotators. This holds true both at the level of whether close-in disk material is present at all, and in analyzing the precise location of the inner disk edge relative to the co-rotation radius amongst the subset of stars with close-in disk material. One interpretation is that disk-locking is unimportant for the IC 348 stars in our sample. Alternatively, if disk-locking does operate, then it must operate on both the slow and rapid rotators, potentially producing both spin-up and spin-down torques, and the transition from the disk-locked state to the disk-released state must occur more rapidly than the stellar contraction timescale.

Subject headings: stars: pre-main-sequence — stars: rotation — stars: circumstellar matter

1. Introduction

Stars are born from the gravitational collapse of dense cores within giant molecular clouds. Conservation of angular momentum would imply that this collapse should produce a star spinning at or near breakup velocity. Actual observations, however, show that young stars rotate much slower than breakup ($\leq 10\%$

¹Department of Physics & Astronomy, Vanderbilt University, 6301 Stevenson Center, Nashville, TN, 37235

²NASA Graduate Student Research Fellow

³Cornell University, Department of Astronomy, 226 Space Sciences Building, Ithaca, NY 14853

⁴Hubble Fellow

⁵Department of Physics, Fisk University, 1000 17th Ave. N., Nashville, TN, 37208

$v_{breakup}$, Hartmann et al. 1986; Bouvier et al. 1986). Where the rest of the angular momentum goes is an important outstanding question.

Circumstellar disks are one important angular momentum reservoir for young stars. During the process of protostellar collapse, a dense core’s highest specific angular momentum material forms a flattened disk which persists for $\sim 2\text{--}3$ Myr (e.g. Lada et al. 2006) to ~ 6 Myr (e.g. Haisch et al. 2001), before it is depleted by accretion onto the star (Bertout et al. 1988; Hartigan et al. 1995), planet formation (Mordasini et al. 2009a,b), outflows (Reipurth et al. 1999; Hartigan et al. 2005), or photoevaporation (Bertoldi 1989).

Theory suggests that magnetic star-disk interactions could play an important role in the star’s early angular momentum evolution (Königl 1991; Shu et al. 1994; Hartmann 2001, 2002). Ghosh & Lamb (1979a,b) and Königl (1991) provided the first analytic descriptions of this process, assuming steady state accretion and a star with a strong magnetic field. In this ‘disk-locking’ picture, angular momentum is transferred from a star to its circumstellar disk via torques arising from interactions between the star’s magnetic field and ionized gas in its circumstellar disk. As the star’s magnetic field weakens with distance, the field couples most strongly to the inner edge of the disk, “locking” the star’s rotation to the Keplerian orbital period at the inner edge of the disk. Shu et al. (1994) extended this theoretical framework by developing the ‘X-wind’ model, in which a magnetically driven wind carries angular momentum away from the “X-point”, where the star and disk’s magnetic fields pinch at the disk’s co-rotation radius. This model, originally assuming a dipolar configuration for the star’s magnetic field, has been generalized by Mohanty & Shu (2008) to include more complex field geometries.

Edwards et al. (1993) and Edwards (1994) provided some of the first observational evidence in support of the disk-locking picture. Analyzing rotation periods measured from stellar light curves, these studies found that stars possessing close-in circumstellar disks (diagnosed via their $H - K$ color excess) were mostly slow rotators, and that stars without $H - K$ excess were fast rotators.

Following these initial findings, many observational studies have searched for signatures of the disk-locking effect by seeking to detect differences between the characteristic rotation rates of stars that possess and lack circumstellar disks, under the assumption that star-disk interactions will force stars with disks to rotate more slowly than those stars that lack disks (e.g. Herbst et al. 2002; Rebull et al. 2004; Covey et al. 2005; Cieza & Baliber 2007). The portrait of a star’s angular momentum evolution that has emerged from these efforts suggests that star-disk interactions lock a star to a slow rotation period ($P \sim 8$ d) matched to the angular velocity of the disk’s inner edge; in this picture stars spin up to become fast rotators ($P \sim 1\text{--}2$ d) only once their disks have begun to dissipate. This picture suggests that slowly rotating young stars should possess disks with smaller inner holes than their faster rotating contemporaries, whose disks have presumably evolved such that star-disk interactions are no longer able to govern the star’s rotation rate.

While most of these observational studies have tested mainly for a statistical correlation between a young star’s rotation period and the presence or absence of a circumstellar disk, a key, generic prediction of disk-locking theories is that disk-locked stars should possess circumstellar disks with inner truncation radii (R_{trunc}) very nearly coincident with their co-rotation radius (R_{co}), the location where a Keplerian orbit within the disk possesses the same angular velocity as the star’s surface. A few studies have attempted detailed comparisons of R_{trunc} vs. R_{co} for samples of young stars where these quantities could be measured or inferred (see Carr 2007, and references therein). For example, Najita et al. (2003) spectroscopically measured R_{trunc} for six stars in Taurus-Auriga, finding that on average $R_{trunc} \approx 0.7 \times R_{co}$. In the context of magnetic star-disk interaction models, this result would suggest that these stars are in fact experiencing active *spin-up* torque from their disks, since the stars would then be coupled to disk material with higher specific angular

momentum than the stars’. However, the sample sizes remain too small to draw robust conclusions. Perhaps most importantly, the range of important parameters—especially stellar rotation period—remains to be fully probed by such analyses. Indeed, the Najita et al. (2003) sample includes only slowly rotating stars with $P_{rot} = 5\text{--}12$ d. Thus, the role of star-disk interaction for more rapidly rotating stars remains an important question.

There are also open questions concerning the universality of the disk locking mechanism. Stassun et al. (1999), Herbst et al. (2002), and Cieza & Baliber (2007), for example, found that the lowest mass stars lack the bimodal rotation period distribution traditionally interpreted as another signature of disk-locking. Additionally, Stassun et al. (2001) investigated the structure of circumstellar disks as a function of rotation period and questioned the idea of a simple dichotomy between disked slow rotators and diskless rapid rotators. From a theoretical standpoint, Matt et al. (2010), also found that models of star-disk interactions incorporating the impact of open field lines were unable to reproduce the observed population of slow rotators. They moreover found that, while the bulk of the stars in their models possessed disks truncated at R_{co} , that did not necessarily imply a zero-torque configuration where the star is “locked” at a constant rotation rate.

In this study, we analyze the properties of 33 stars in IC 348 to test the agreement between their rotation periods and the Keplerian orbital periods at the inner edges of their circumstellar disks. In particular, we seek to test two implications of the commonly presented picture of the disk locking phenomena: (1) How do R_{trunc} and R_{co} compare for a well populated ensemble of circumstellar disks, and (2) do fast rotators possess disks with $R_{trunc} \gg R_{co}$, as expected if the disks around fast rotators have evolved to the point that star-disk interactions no longer govern their host star’s rotation rate? In Sec. 2, we describe the fundamentals of the test, as well as the parameters needed (stellar properties, disk properties inferred from photometry, and the model grid). We then apply the test and report the findings in Sec. 3. We discuss the implications in Sec. 4 and conclude with a summary in Sec. 5.

2. Methods

We aim to conduct a quantitative test of a central prediction of disk locking theories: Does a young star rotate with a period equal to the Keplerian orbital period of its inner disk? To perform this test, we define two characteristic locations within the circumstellar disk: the distance from the star to the disk’s inner edge, R_{trunc} , and R_{co} , the radius at which the Keplerian angular velocity in the disk equals the star’s angular velocity (Ghosh & Lamb 1979b; Shu et al. 1994). R_{co} is calculated for each star as:

$$R_{co} = (GM_{\star}P_{rot}^2/4\pi^2)^{1/3} \quad (1)$$

where M_{\star} and P_{rot} are the star’s mass and rotation period, respectively.

To measure the truncation radius of each young star’s circumstellar disk, we analyze the amount of excess emission detected from each star at near- and mid-infrared wavelengths, arising from warm dust in the inner circumstellar disk. Specifically, we compare mid-infrared photometry from the Spitzer Space Telescope, as well as ground-based optical and near-infrared observations, to synthetic spectral energy distributions (SEDs) computed from a grid of 200,000 Monte-Carlo models covering a wide range of parameter space. We conduct this analysis on young stars in IC 348, a nearby, young cluster in the Perseus star forming region. This compact, optically visible region is amenable to photometric surveys at optical wavelengths, enabling efficient measurements of stellar rotation via star-spot modulation of stellar light curves, and the construction of SEDs sampling the short wavelengths dominated by the stellar photosphere, as well as the longer wavelengths dominated by the circumstellar disk.

2.1. Photometry from the Literature

In this study, we make use of the SED measurements compiled by Lada et al. (2006) (L06) in their study of circumstellar disks in IC 348. L06 combined ground-based broadband RIJHK measurements with mid-IR photometry from the Infrared Array Camera (IRAC) and Multiband Imaging Photometer (MIPS) on the Spitzer Space Telescope to produce SEDs for ~ 300 stars previously identified as cluster members by Luhman et al. (2003). The L06 SEDs span $0.5\text{--}24\ \mu\text{m}$, providing good sensitivity to emission from the stellar photosphere as well as the inner circumstellar disk. L06 reported the broadband photometry in magnitudes; we converted these into flux units using standard passband zeropoints (Cousins 1976; Cohen et al. 2003; Fazio et al. 2004), which are summarized in Table 1.

2.2. Stellar Properties

Calculating R_{co} for each star in our sample requires measurements of P_{rot} , M_* , and R_* (see Eq. 1 above). To infer each star’s mass and radius, we adopt the T_{eff} , L_{bol} and A_V values determined for these stars by Luhman et al. (2003). Stellar masses were inferred for each star by comparing the measured T_{eff} s and L_{bol} s to pre-main sequence evolutionary models calculated by D’Antona & Mazzitelli (1997)(DM97). We calculate stellar radii using the fundamental Stephan-Boltzmann law, which relates the star’s luminosity (L_*) to a given radius (R_*) and T_{eff} : $L_* = 4\pi R_*^2 \sigma T_{eff}^4$, where σ is the Stefan-Boltzmann constant. The full set of adopted and inferred parameters for each star are presented in Table 2. Typical errors in M_* and R_* are derived from errors in T_{eff} and L_* , with typical T_{eff} errors of half a spectral subtype (± 82.5 K for M-type, ± 140 K for K-type), and typical errors of ≈ 0.3 in $\log L_*$ (e.g. Hartmann 2001). We adopt rotation periods from the catalog presented by Cieza & Baliber (2006), who measured P_{rot} due to starspot modulation of each star’s light curve, from their multi-epoch I_C photometry of IC 348. To identify stars with circumstellar disks, we applied a $[3.6]\text{--}[8.0] > 0.7$ color cut as adopted by Cieza & Baliber (2006) to the stars in the L06 catalog (see Fig. 1). For the low-mass stars under consideration here, this color cut ensures that dusty disk material is present within ~ 1 AU of our sample stars.

This leaves 33 stars with the requisite data for our study. For 27 of these we are able to determine the disk properties via SED fitting (see below). These are summarized in Table 2.

2.3. SED Models

We make use of a pre-computed grid of models, generated by Robitaille et al. (2006) (henceforth R06), to compare with photometry for stars in this study. This grid builds upon previous work done by Whitney et al. (2003a,b) (hereafter W03a, W03b), by calculating the temperature structure of circumstellar disks of young stellar objects (YSOs). W03a generated two-dimensional radiative transfer models of Class I YSOs, while W03b presented model SEDs, polarizations, and images for an evolutionary sequence of YSOs from Class 0 to Class III. The W03a/W03b code uses Monte Carlo radiative equilibrium to generate model SEDs for YSOs, following the trajectory of photon packets emitted from a central stellar source into a disk and modeling their absorption, re-emission, and/or scattering (Bjorkman & Wood 2001). This method yields a model temperature structure specific to the parameters describing the star (e.g., T_{eff} and R_*) and its disk (e.g., R_{trunc} , M_* , and scale-height).

The R06 model grid consists of SED models calculated using the W03a algorithm, and covering a wide

range of masses (from 0.1 to 50 M_{\odot}) and stages of YSO evolution. R06 characterized each model using 16 stellar, disk, and envelope parameters; the most pertinent to this study include stellar mass, temperature, and radius, as well as disk mass and R_{trunc} . The grid consists of 200,000 SEDs computed at ten different angles (ranging from near face-on at 18° , to near edge-on at 87°), resulting in a comprehensive set of SEDs suitable to comparing with actual YSO photometry. By comparing these synthetic SEDs with the observed SEDs we have assembled for our sample, we can infer the physical properties of each star’s disk.

We used the R06 model grid to identify those models which reproduce each IC 348 member’s observed SED. We limit each star’s acceptable fits, however, to those models with distances (315 ± 30 pc) comparable to those measured for most IC 348 members. The initial matches were further screened on the basis of goodness of fit with the observed SED, agreement with the T_{eff} value reported in the literature for each star, and the implied A_V and disk mass:

- **T_{eff} filter** — We retain only those models with T_{eff} within ± 500 K of the value reported in the literature from previous spectroscopy-based determinations.;
- **χ^2 filter** — A χ^2 metric is applied to ensure goodness-of-fit, such that the models selected possessed $\chi^2 \leq \chi_{best}^2 + 9.21$. This value corresponds to a 99% confidence level for two model parameters of interest in our SED fitting (Press et al. 1992), R_{trunc} and M_{disk} (see below).
- **A_V filter** — Previous work generally found A_V for IC 348 members to be modest, rarely larger than ~ 5 mag (e.g. L06). Therefore, our SED fitting results with $A_V \geq 10$ were eliminated to remove models with excessive combined interstellar and stellar extinction. In most cases, models with artificially large A_V were already eliminated by the T_{eff} filter above.
- **M_{disk} filter** — Models lacking sufficiently massive disks ($M_{disk} \leq 10^{-4} M_{\odot}$) are also removed. Such low-mass disks are rarely seen in sub-mm surveys (Andrews & Williams 2005), and are unlikely to be capable of sustaining significant star-disk interaction.

Of the 33 stars initially in our sample, six could not be matched to models in the R06 grid which satisfy all of the above criteria (star IDs 6, 21, 41, 61, 140, and 182; refer to Table 3). In most cases this was because the best-fit SED models required very low disk masses ($M_{disk} < 10^{-4} M_{\odot}$). We therefore exclude these stars from our subsequent analysis. The results of the model vs. observed SED comparisons for the remaining 27 stars are discussed in § 3, with summaries of the SED fitting results for three representative stars shown in Figs. 2–4.

3. Results

3.1. Inferred Disk Truncation, Co-rotation, and Dust Sublimation Radii

We have inferred R_{trunc} for each star by computing the mean R_{trunc} of the full suite of R06 models which acceptably reproduce that star’s SED and meet each of the criteria outlined above. To provide context for these mean R_{trunc} values, we calculated the ratio between each star’s R_{trunc} and its co-rotation and dust-sublimation radii (R_{co} and R_{sub} , respectively). The first of these ratios, R_{trunc}/R_{co} , is of course the principal quantity that we seek to test, as $R_{trunc}/R_{co} \approx 1$ is predicted by most disk-locking theories (see §1).

We also compute R_{trunc}/R_{sub} , which indicates if the R_{trunc} value returned by the SED model fits corresponds to the true inner edge of the circumstellar disk. Magnetic star-disk interaction requires the

stellar magnetic field lines to connect to ionized gas in the circumstellar disk. It is therefore important to note that the observed SEDs used here, based on broadband fluxes, strictly speaking trace only the spatial extent of a disk’s dust. However, dust that is sufficiently close to the stellar surface is expected to be destroyed via sublimation. This effect is included in the R06 SED model grid; if a disk would otherwise extend inward of R_{sub} , the disk is forced to have $R_{trunc} = R_{sub}$. R_{sub} is given by (Tuthill et al. 2001; D’Alessio et al. 2004; Whitney et al. 2003a,b): $R_{sub} = R_{\star} \times (T_{sub}/T_{eff})^{-2.1}$ where T_{sub} is the temperature at which dust is destroyed by photoevaporation (the R06 grid assumes $T_{sub} = 1600$ K).

In cases for which we find $R_{trunc} = R_{sub}$, we assume that the dust has been truncated by sublimation, a process which would not remove the gas (e.g. Najita et al. 2003; Eisner et al. 2005). Therefore, in these cases we assume that the gas in the disk in fact extends closer to the star than inferred from the observed SED; the inferred R_{trunc} in these cases is therefore an upper limit. Conversely, in cases for which we find $R_{trunc} > R_{sub}$, some other process may be responsible for clearing out the inner portion of the disk, and therefore we assume that the inner gas is cleared out as well (e.g. Isella et al. 2009).

Fig. 5 shows the R_{trunc}/R_{co} and R_{trunc}/R_{sub} ratios for our entire sample. We immediately identify two distinct populations of stars: One group with $R_{trunc} \gg R_{co}$ and $R_{trunc} \gg R_{sub}$ (32% of the final sample), and a second group with $R_{trunc} \approx R_{co}$ (68% of the sample).

Since R_{co} is generally the location of “action” in most magnetic star-disk interaction models (Shu et al. 1994; Mohanty & Shu 2008; Matt et al. 2010), the first group represents stars for which a magnetic star-disk interaction is most likely not important. With physically very large R_{trunc} , far beyond R_{co} , these stars evidently harbor disks that have evolved significantly and no longer present substantial disk material within reach of the stellar magnetosphere; we refer to these stars as “effectively diskless”. In contrast, the latter group represents stars with substantial disk material situated at or very near to the location of potential star-disk interaction. While the precise location of the inner-disk edge relative to R_{co} requires a detailed examination of possible dust sublimation effects (which we do below), as discussed above the effect of such dust sublimation will be to imply a true R_{trunc} that is even closer to the star than what we have inferred, and for which we might expect active interaction between the disk and the stellar magnetosphere to be even more likely. Therefore, we refer to this group of stars as “potentially disk-locked”. We discuss the implications of these two groups in more detail below.

3.2. Comparison of Potentially Disk-Locked and Effectively Diskless Stars

Figure 6 shows the location of these IC 348 members within the HR diagram, with tracks and isochrones calculated by DM97 overlaid for comparison. The IC 348 members analyzed here possess HR diagram locations consistent with 1–2 Myr isochrones, with implied masses of $0.7 M_{\odot}$ or below. There is no clear difference between the ages and masses of the members of the potentially disk-locked and effectively diskless groups: this visual conclusion is supported by 1D and 2D two sided K-S tests, which indicate that the ages and masses of the stars in the two groups are consistent with shared parent populations at 94% and 74% confidence levels (1D) and 52% (2D). We also applied a two-sided K-S test on the rotation period distributions for the potentially disk-locked and effectively diskless groups (see Fig. 7). The K-S test in this case returns a probability of 0.74, and as such we cannot reject the null hypothesis that the two distributions are drawn from the same parent distribution.

4. Discussion

Our SED modeling provides the first detailed investigation of how the structure of circumstellar disks around IC 348 members does or does not influence the star’s rotation rate. Specifically, these measurements provide leverage to address the two questions motivating this study: 1) how do the inner truncation radii and co-rotation radii compare for a well populated ensemble of circumstellar disks, and 2) do fast rotators possess circumstellar disks with inner radii larger than co-rotation, as expected if the disks around fast rotators have evolved to the point that star-disk interactions no longer govern their host star’s rotation rate? We address each of these questions in turn.

4.1. Are circumstellar disks truncated at co-rotation?

Traditionally, the condition $R_{\text{trunc}} \approx R_{\text{co}}$ has been assumed as a fundamental requirement for a star to be in a fully disk-locked state, where a quasi-steady-state configuration of the star-disk interaction exerts a braking torque on the star that counter-balances the star’s tendency to spin up as it contracts, and thus maintains a roughly constant stellar rotation period for the lifetime of the disk. For example, in the context of the bimodal distribution of rotation periods reported by Herbst and collaborators in the ONC (e.g. Herbst et al. 2002), the slow rotators have been interpreted as those in an actively “disk-locked” state while the rapid rotators have been interpreted as “disk-released,” presumably due to the loss of their disks. These interpretations have generally been made on the basis of near- and mid-IR colors as functions of stellar rotation period, not on an assessment of the $R_{\text{trunc}}/R_{\text{co}}$ condition on a star by star basis.

Our detailed SED analysis reveals that the majority (70%) of the stars in our sample have clear evidence for $R_{\text{trunc}} \approx R_{\text{co}}$ (Fig. 5). As these potentially disk-locked stars constitute the majority of our sample, it does appear that most stars in IC 348 are consistent with the zeroth order prediction of theoretical models of angular momentum transfer via star-disk interactions.

However, assessing whether the potentially disk-locked stars are experiencing a *braking* torque from any presumed star-disk interaction is made more subtle by the complicating effects of dust sublimation on the determination of the disk’s true R_{trunc} . As shown in Fig. 5, while both the slow and rapid rotators in the potentially disk-locked group are similarly distributed along the vertical axis (i.e., both the slow and rapid rotators have disks consistent with $R_{\text{trunc}} = R_{\text{co}}$, within error), their distributions along the horizontal axis are detectably different. The rapid rotators are very strongly clustered at precisely $R_{\text{trunc}}/R_{\text{sub}} = 1$ (scatter in $R_{\text{trunc}}/R_{\text{sub}}$ of less than 1%), which is the hard minimum that any of our SED models can attain because (by definition) dust is destroyed by sublimation interior to this radius. In contrast, the slow rotators show a larger spread of $\sim 15\%$ in $R_{\text{trunc}}/R_{\text{sub}}$. Moreover, most of the slow rotators’ disks are mildly inconsistent with $R_{\text{trunc}} = R_{\text{sub}}$, requiring $R_{\text{trunc}} > R_{\text{sub}}$ with greater than 1σ confidence. Taken as a group, the rapid rotators show a high likelihood of possessing a mean $R_{\text{trunc}}/R_{\text{sub}} = 1$, while the likelihood that the slow rotators possess a mean $R_{\text{trunc}}/R_{\text{sub}} = 1$ is less than 0.1%.

We interpret the uniform pile-up of fast rotators at $R_{\text{trunc}}/R_{\text{sub}} = 1$ to mean that our SED modeling is not sensitive to the true inner edge of the fast rotators’ disks, which likely extend inward of R_{sub} and perhaps significantly inward of R_{co} as well (though we cannot verify the latter). In contrast, the $R_{\text{trunc}}/R_{\text{sub}}$ ratios that we observe for the slow rotators are significantly larger than 1. Therefore we regard the R_{trunc} for the slow rotators in general to correspond to true R_{trunc} measurements, and thus we can conclude with greater confidence that these stars truly have disks consistent with $R_{\text{trunc}}/R_{\text{co}} = 1$.

If the potentially disk-locked stars in our sample are in fact experiencing angular momentum interactions with their disks, the above findings could imply that the slow rotators are slow precisely because they satisfy the $R_{trunc}/R_{co} = 1$ condition, while the fast rotators are fast because they tend to possess disks with $R_{trunc}/R_{co} < 1$. (To be clear, our results do not demonstrate that $R_{trunc}/R_{co} < 1$ for the rapid rotators in the potentially disk-locked group, but such an interpretation would be consistent with our findings above.) Recent theoretical work complicates such a straightforward interpretation, however. Matt et al. (2010) have demonstrated that the condition $R_{trunc}/R_{co} \approx 1$ can in fact transpire for a very wide range of star/disk parameters and a wide range of star-disk torque configurations. Indeed, in those calculations, relatively small deviations from $R_{trunc}/R_{co} = 1$ can result in large differences in the magnitude and/or the sign of the torque experienced by the star. For example, in the case of strong magnetic coupling to the disk (e.g., $\beta = 0.01$), significant field twisting occurs for R_{trunc} deviations of less than 1% from R_{co} . The R_{trunc}/R_{co} that we have determined for potentially disk-locked stars are not sufficiently precise to make such distinctions.

Nonetheless, the findings of Matt et al. (2010) do still predict that disks with smaller R_{trunc}/R_{co} will in general result in more positive stellar torques. Thus, if the potentially disk-locked stars in our sample are in fact disk-locked, the implication is that the rapid rotators are likely experiencing systematically more positive torques. More generally, under the disk-locking hypothesis, our results are most consistent with an interpretation in which the stars are currently experiencing disk torques spanning a large range of magnitude, and perhaps in sign.

4.2. Do fast rotators possess (dust) disks with larger inner holes?

As commonly envisaged, magnetic star-disk interactions force the star to rotate at the Keplerian velocity of the close-in inner disk. Over time, however, the disk’s inner hole grows¹ as the disk evolves and begins to dissipate; eventually star-disk interactions are too weak to couple the star to the anemic inner disk, and the star spins up as it completes its pre-main sequence contraction. This picture would predict that slowly rotating stars will be locked to disks with $R_{trunc} \approx R_{co}$, while rapidly rotating stars would be associated with disks with $R_{trunc} \gg R_{co}$ (Edwards et al. 1993; Edwards 1994; Rebull et al. 2006; Cieza & Baliber 2007). To test this picture, we can compare the P_{rot} distributions for the potentially disk-locked and effectively diskless stars in our sample.

Interestingly, we find slow and rapid rotators in roughly equal numbers among the potentially disk-locked stars. This suggests that the common interpretation, wherein fast rotators result from stellar spin-up following the cessation of disk-locking, may need to be modified to allow for the existence of rapidly rotating stars with close-in disks. Indeed, both slow and rapid rotators amongst the potentially disk-locked stars in our sample at least approximately satisfy the condition $R_{trunc} \approx R_{co}$. As discussed above, the rapid rotators in the potentially disk-locked group may in fact possess disks with $R_{trunc} < R_{co}$, however this only strengthens the conclusion that rapid rotators do not possess disks with systematically larger inner holes compared to the slow rotators.

The effectively diskless stars in our sample are very unlikely to be experiencing significant torques from their disks. Interestingly, however, the rotation period distribution of these stars is nonetheless very similar

¹While other models of disk evolution that do not predict a widening inner-disk hole do exist (e.g., homologous depletion; (Currie et al. 2009; Currie & Sicilia-Aguilar 2011), ‘inside-out’ disk evolution is the most commonly invoked (e.g. Barsony et al. 2005).

to that of the potentially disk-locked stars (see §3.2). Presuming that the effectively diskless stars formerly possessed robust inner disks like their present-day potentially disk-locked counterparts, this implies that their disk properties have evolved significantly while their rotational properties have remained unchanged. If the currently effectively diskless stars are furthermore presumed to have formerly been in a disk-locked state, then the timescale for transitioning from the disk-locked to the disk-released state must be shorter than the timescale on which the stars would spin up due to pre-main-sequence contraction. This conclusion is consistent with previous estimates of disk evolution timescales, which find timescales of $\sim 0.1\text{--}1$ Myr for disk evolution processes (Currie & Sicilia-Aguilar 2011; Muzerolle et al. 2010), compared to the ~ 3 Myr spin-up timescale predicted by the DM97 PMS evolutionary models for $0.4M_{\odot}$ stars (the average mass of our sample) at 1 Myr. This is also consistent with the statistics of our sample: 1/3 of our sample are “effectively diskless”, implying a disk evolution timescale (assuming the nominal age of 1 Myr typically adopted for IC 348) of $\sim 1/3 \times 1 \text{ Myr} = \sim 0.3$ Myr, in agreement with aforementioned timescale estimates.

5. Summary and Conclusions

We have analyzed the circumstellar disks around a sample of 33 stars in IC 348 with known rotation periods, in order to assess in detail whether the inner edge of each star’s circumstellar disk (R_{trunc}) is consistent with being at the co-rotation radius from the star (R_{co}), as predicted by disk-locking theory. We compare stellar photometry from the Spitzer Space Telescope to a grid of 200,000 pre-computed star+disk radiative transfer models, and compare the implied R_{trunc} of the best fitting SED models to each star’s calculated R_{co} . The principal findings of this study are as follows:

- We find two populations of stars: a “potentially disk-locked group” with inner-disk radii located at $R_{trunc}/R_{co} \approx 1$ (68% of the sample), and an “effectively diskless” group whose inner-disk radii are significantly larger, with $R_{trunc}/R_{co} \gg 1$ and thus beyond the reach of disk-locking (32% of the sample).
- Both fast and slow rotators in the potentially disk-locked group possess dust disks with R_{trunc}/R_{co} values consistent with 1. This finding is contrary to previous suggestions that slowly-rotating stars will possess close-in disks that facilitate strong star-disk interactions, while fast rotators will possess more evolved disks with inner radii that are sufficiently large so that they are no longer amenable to significant star-disk interactions. The general agreement between the each star’s R_{trunc} and R_{co} may be taken to suggest that star disk-interactions do indeed play a role in these stars’ angular momentum evolution. However, under this hypothesis, the lack of a clear distinction between the R_{trunc} inferred for the disks around fast and slow rotators would imply that star-disk interactions influence the rotation rate of the fast rotators as well, not only the slow rotators whose periods disk locking is most commonly invoked to explain.
- Stars in both the potentially disk-locked and effectively diskless groups, whose disks we interpret as being in significantly different evolutionary states, possess statistically identical rotation period distributions. If the potentially disk-locked stars are presumed to currently be in a disk-locked state, and if the effectively diskless stars are presumed to previously have been in a similarly disk-locked state, this suggests that disks evolve more quickly than the stellar spin-up timescale resulting from pre-main-sequence contraction.

In summary, while our findings may be interpreted within the context of a presumed disk-locking mechanism, invoking the disk-locking hypothesis is not necessitated by the stars in our IC 348 study sample. We do not find obvious differences in the disk truncation radii of slow rotators vs. rapid rotators. This holds true both at the level of whether close-in disk material is present at all, and in analyzing the precise location of the inner disk edge relative to the co-rotation radius amongst the subset of stars with close-in disk material. These results may therefore imply that the disk-locking phenomenon is not operative in these stars. Alternatively, if disk-locking does operate, then our findings imply that (a) its observational signature is more complex than the simple portrait of slowly rotating disk-locked stars and rapidly rotating non-disk-locked stars, and (b) the transition from the disk-locked state to the disk-released state must occur more rapidly than the stellar contraction timescale.

We acknowledge and thank Sean Matt for helpful and insightful discussions of angular momentum transfer via star-disk interactions. This research has made use of NASA’s Astrophysics Data System Bibliographic Services, the SIMBAD database, operated at CDS, Strasbourg, France, and photometry acquired as part of the Two Micron All Sky Survey. The Two Micron All Sky Survey was a joint project of the University of Massachusetts and the Infrared Processing and Analysis Center (California Institute of Technology). The University of Massachusetts was responsible for the overall management of the project, the observing facilities and the data acquisition. The Infrared Processing and Analysis Center was responsible for data processing, data distribution and data archiving. TSL gratefully acknowledges the support provided for this work by NASA through the NASA Graduate Student Research Program (GSRP). KRC gratefully acknowledges support provided for this work by NASA through Hubble Fellowship grant HST-HF-51253.01-A awarded by the STScI, which is operated by the AURA, Inc., for NASA, under contract NAS 5-26555, and by the Spitzer Space Telescope Fellowship Program, through a contract issued by the Jet Propulsion Laboratory, California Institute of Technology under a contract with NASA.

REFERENCES

- Andrews, S. M. & Williams, J. P. 2005, *ApJ*, 631, 1134
- Barsony, M., Ressler, M. E., & Marsh, K. A. 2005, *ApJ*, 630, 381
- Bertoldi, F. 1989, *ApJ*, 346, 735
- Bertout, C., Basri, G., & Bouvier, J. 1988, *ApJ*, 330, 350
- Bjorkman, J. E. & Wood, K. 2001, *ApJ*, 554, 615
- Bouvier, J., Bertout, C., Benz, W., & Mayor, M. 1986, *A&A*, 165, 110
- Carr, J. S. 2007, in *IAU Symposium*, Vol. 243, *IAU Symposium*, ed. J. Bouvier & I. Appenzeller, 135–146
- Cieza, L. & Baliber, N. 2006, *ApJ*, 649, 862
- . 2007, *ApJ*, 671, 605
- Cohen, M., Wheaton, W. A., & Megeath, S. T. 2003, *AJ*, 126, 1090
- Cousins, A. W. J. 1976, *MmRAS*, 81, 25

- Covey, K. R., Greene, T. P., Doppmann, G. W., & Lada, C. J. 2005, *AJ*, 129, 2765
- Currie, T., Lada, C. J., Plavchan, P., Robitaille, T. P., Irwin, J., & Kenyon, S. J. 2009, *ApJ*, 698, 1
- Currie, T. & Sicilia-Aguilar, A. 2011, *ApJ*, 732, 24
- D’Alessio, P., Calvet, N., Hartmann, L., Muzerolle, J., & Sitko, M. 2004, in *IAU Symposium*, Vol. 221, *Star Formation at High Angular Resolution*, ed. M. G. Burton, R. Jayawardhana, & T. L. Bourke, 403–+
- D’Antona, F. & Mazzitelli, I. 1997, *Memorie della Societa Astronomica Italiana*, 68, 807
- Edwards, S. 1994, *Revista Mexicana de Astronomia y Astrofisica*, vol. 29, 29, 35
- Edwards, S., Strom, S. E., Hartigan, P., Strom, K. M., Hillenbrand, L. A., Herbst, W., Attridge, J., Merrill, K. M., Probst, R., & Gatley, I. 1993, *AJ*, 106, 372
- Eisner, J. A., Hillenbrand, L. A., White, R. J., Akeson, R. L., & Sargent, A. I. 2005, *ApJ*, 623, 952
- Fazio, G. G., Hora, J. L., Allen, L. E., Ashby, M. L. N., Barmby, P., Deutsch, L. K., Huang, J., Kleiner, S., Marengo, M., Megeath, S. T., Melnick, G. J., Pahre, M. A., Patten, B. M., Polizotti, J., Smith, H. A., Taylor, R. S., Wang, Z., Willner, S. P., Hoffmann, W. F., Pipher, J. L., Forrest, W. J., McMurty, C. W., McCreight, C. R., McKelvey, M. E., McMurray, R. E., Koch, D. G., Moseley, S. H., Arendt, R. G., Mentzell, J. E., Marx, C. T., Losch, P., Mayman, P., Eichhorn, W., Krebs, D., Jhabvala, M., Gezari, D. Y., Fixsen, D. J., Flores, J., Shakoorzadeh, K., Jungo, R., Hakun, C., Workman, L., Karpati, G., Kichak, R., Whitley, R., Mann, S., Tollestrup, E. V., Eisenhardt, P., Stern, D., Gorjian, V., Bhattacharya, B., Carey, S., Nelson, B. O., Glaccum, W. J., Lacy, M., Lowrance, P. J., Laine, S., Reach, W. T., Stauffer, J. A., Surace, J. A., Wilson, G., Wright, E. L., Hoffman, A., Domingo, G., & Cohen, M. 2004, *ApJS*, 154, 10
- Ghosh, P. & Lamb, F. K. 1979a, *ApJ*, 232, 259
- . 1979b, *ApJ*, 234, 296
- Haisch, Jr., K. E., Lada, E. A., & Lada, C. J. 2001, *ApJ*, 553, L153
- Hartigan, P., Edwards, S., & Ghandour, L. 1995, *ApJ*, 452, 736
- Hartigan, P., Heathcote, S., Morse, J. A., Reipurth, B., & Bally, J. 2005, *AJ*, 130, 2197
- Hartmann, L. 2001, *Pre-Main Sequence Evolution of Low-Mass Stars*
- . 2002, *On Disk Braking of T Tauri Rotation*
- Hartmann, L., Hewett, R., Stahler, S., & Mathieu, R. D. 1986, *ApJ*, 309, 275
- Herbst, W., Bailer-Jones, C. A. L., Mundt, R., Meisenheimer, K., & Wackermann, R. 2002, *A&A*, 396, 513
- Isella, A., Carpenter, J. M., & Sargent, A. I. 2009, *ApJ*, 701, 260
- Königl, A. 1991, *ApJ*, 370, L39
- Lada, C. J., Muench, A. A., Luhman, K. L., Allen, L., Hartmann, L., Megeath, T., Myers, P., Fazio, G., Wood, K., Muzerolle, J., Rieke, G., Siegler, N., & Young, E. 2006, *AJ*, 131, 1574

- Luhman, K. L., Stauffer, J. R., Muench, A. A., Rieke, G. H., Lada, E. A., Bouvier, J., & Lada, C. J. 2003, *ApJ*, 593, 1093
- Matt, S. P., Pinzón, G., de la Reza, R., & Greene, T. P. 2010, *ApJ*, 714, 989
- Mohanty, S. & Shu, F. H. 2008, *ApJ*, 687, 1323
- Mordasini, C., Alibert, Y., & Benz, W. 2009a, *A&A*, 501, 1139
- Mordasini, C., Alibert, Y., Benz, W., & Naef, D. 2009b, *A&A*, 501, 1161
- Muzerolle, J., Allen, L. E., Megeath, S. T., Hernández, J., & Gutermuth, R. A. 2010, *ApJ*, 708, 1107
- Najita, J., Carr, J. S., & Mathieu, R. D. 2003, *ApJ*, 589, 931
- Press, W. H., Teukolsky, S. A., Vetterling, W. T., & Flannery, B. P. 1992, *Numerical Recipes In FORTRAN. The Art Of Scientific Computing* (Cambridge University Press)
- Rebull, L. M., Stauffer, J. R., Megeath, S. T., Hora, J. L., & Hartmann, L. 2006, *ApJ*, 646, 297
- Rebull, L. M., Wolff, S. C., & Strom, S. E. 2004, *AJ*, 127, 1029
- Reipurth, B., Yu, K. C., Rodríguez, L. F., Heathcote, S., & Bally, J. 1999, *A&A*, 352, L83
- Robitaille, T. P., Whitney, B. A., Indebetouw, R., Wood, K., & Denzmore, P. 2006, *ApJS*, 167, 256
- Shu, F., Najita, J., Ostriker, E., Wilkin, F., Ruden, S., & Lizano, S. 1994, *ApJ*, 429, 781
- Stassun, K. G., Mathieu, R. D., Mazeh, T., & Vrba, F. J. 1999, *AJ*, 117, 2941
- Stassun, K. G., Mathieu, R. D., Vrba, F. J., Mazeh, T., & Henden, A. 2001, *AJ*, 121, 1003
- Tuthill, P. G., Monnier, J. D., & Danchi, W. C. 2001, *Nature*, 409, 1012
- Whitney, B. A., Wood, K., Bjorkman, J. E., & Cohen, M. 2003a, *ApJ*, 598, 1079
- Whitney, B. A., Wood, K., Bjorkman, J. E., & Wolff, M. J. 2003b, *ApJ*, 591, 1049

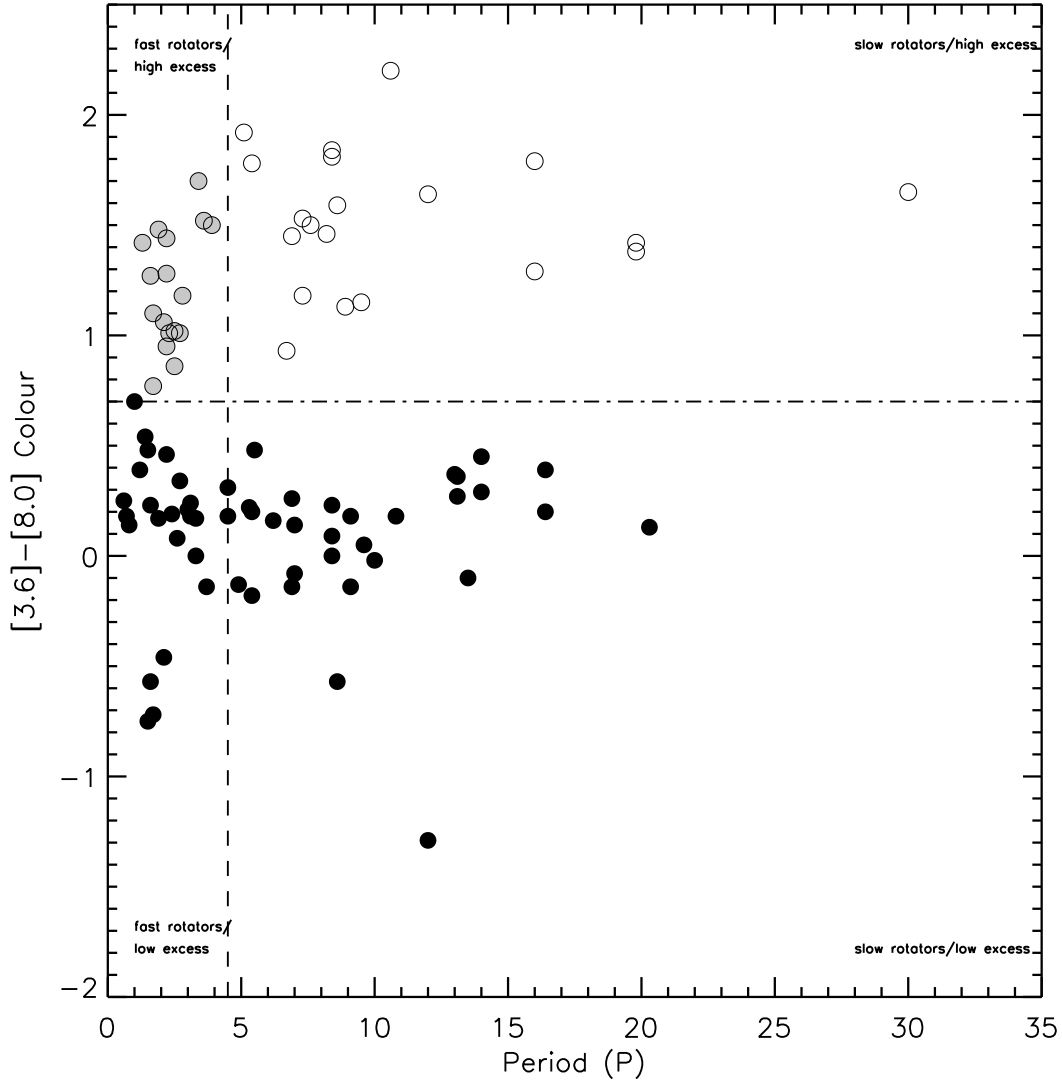


Fig. 1.— IRAC [3.6]-[8.0] color vs. rotation period for IC 348 members. The horizontal dashed line shows the IRAC color cut ($[3.6]-[8.0] > 0.7$) used to identify IC 348 members with substantial circumstellar disks. Periods are taken from the Lada et al. (2006); Cieza & Baliber (2006); Luhman et al. (2003) catalogues: the vertical dashed line indicates a period of 4.5 days, used to separate the sample of stars with disks into subsets of fast rotators ($P_{rot} < 4.5$ days; light grey filled circles) and slow rotators ($P_{rot} > 4.5$ days; empty circles). See electronic edition of the journal for a coloured version of this figure.

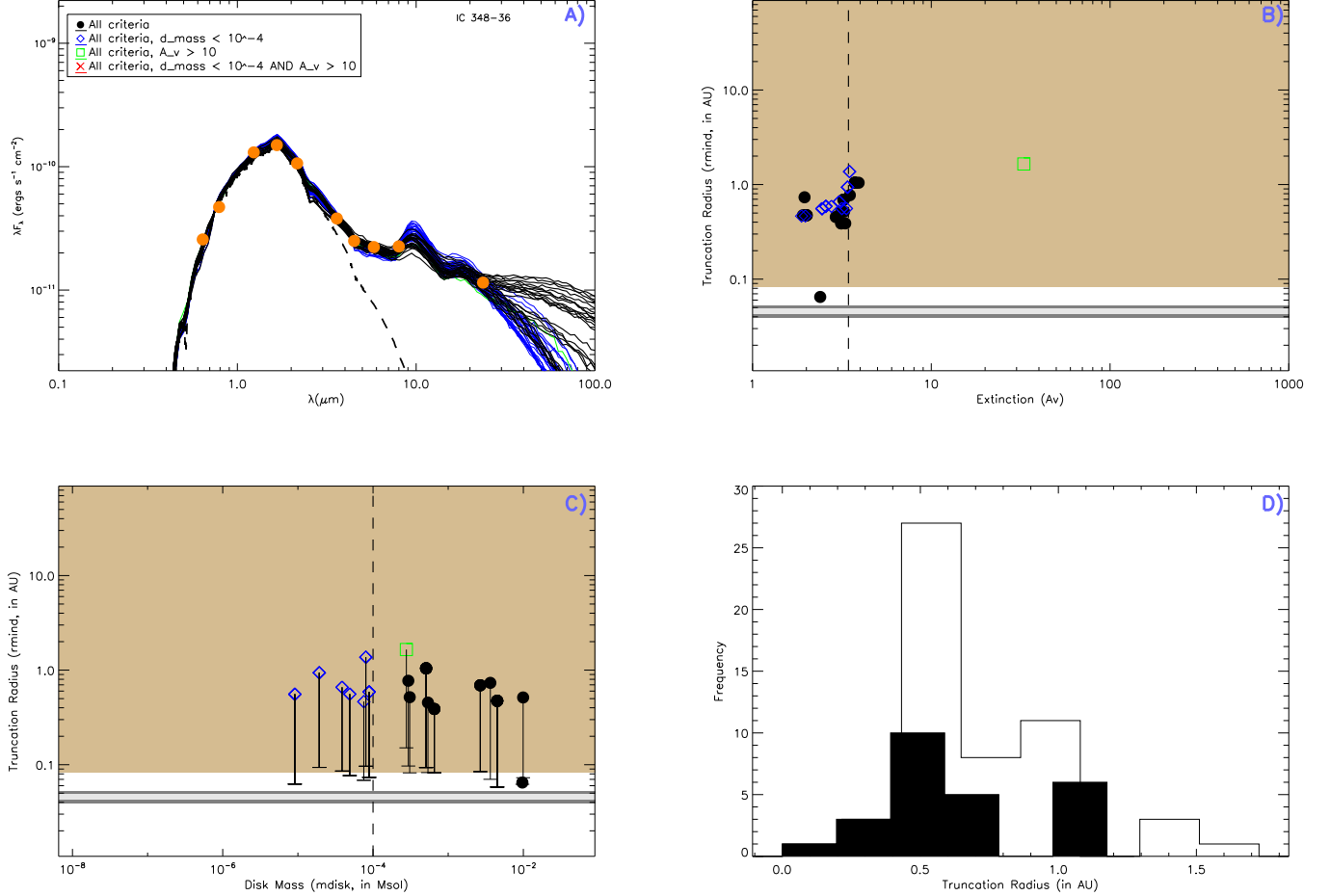


Fig. 2.— SED fitting results for IC 348 36, an example of a star whose model fit predicts $R_{trunc} \gg R_{co}$, and $R_{trunc} \gg R_{sub}$. **Panel A)** Photometric SED (detections shown as yellow filled circles; upper limits as yellow arrows) compared to an artificially reddened Phoenix stellar atmosphere with the same T_{eff} (dashed line) and SED fits from the R06 model grid: black lines show R06 model SEDs meeting all criteria outlined in § 2.3, with colored lines showing models that fail one of those criteria (see legend in panel). **Panels B and C)** Location of model fits in R_{trunc} vs. M_{disk} or A_V parameter space. Black points indicate models meeting all criteria in § 2.3. Models failing the limits on M_{disk} & A_V are shown as blue diamonds and green squares, respectively, with models failing both criteria shown as red crosses. Lower “error” bars indicate the distance between R_{trunc} and R_{sub} (at each model’s T_{eff}). Vertical dashed lines in panels B & C show the M_{disk} limit and the A_V value reported for this star in the literature, respectively. The domain where $R > R_{sub}$ is indicated with a mocha background; light grey bars show the range of possible R_{co} s assuming a 50% uncertainty in M_* , with dark grey bands indicating the range of possible R_{co} s assuming a conservative 100% uncertainty in M_* . **Panel D)** Distribution of R_{trunc} values for all R06 models satisfying the basic χ^2 criteria (open histogram), and for models meeting all criteria (filled histogram). Coloured plots for all sources are available in the electronic edition of the journal.

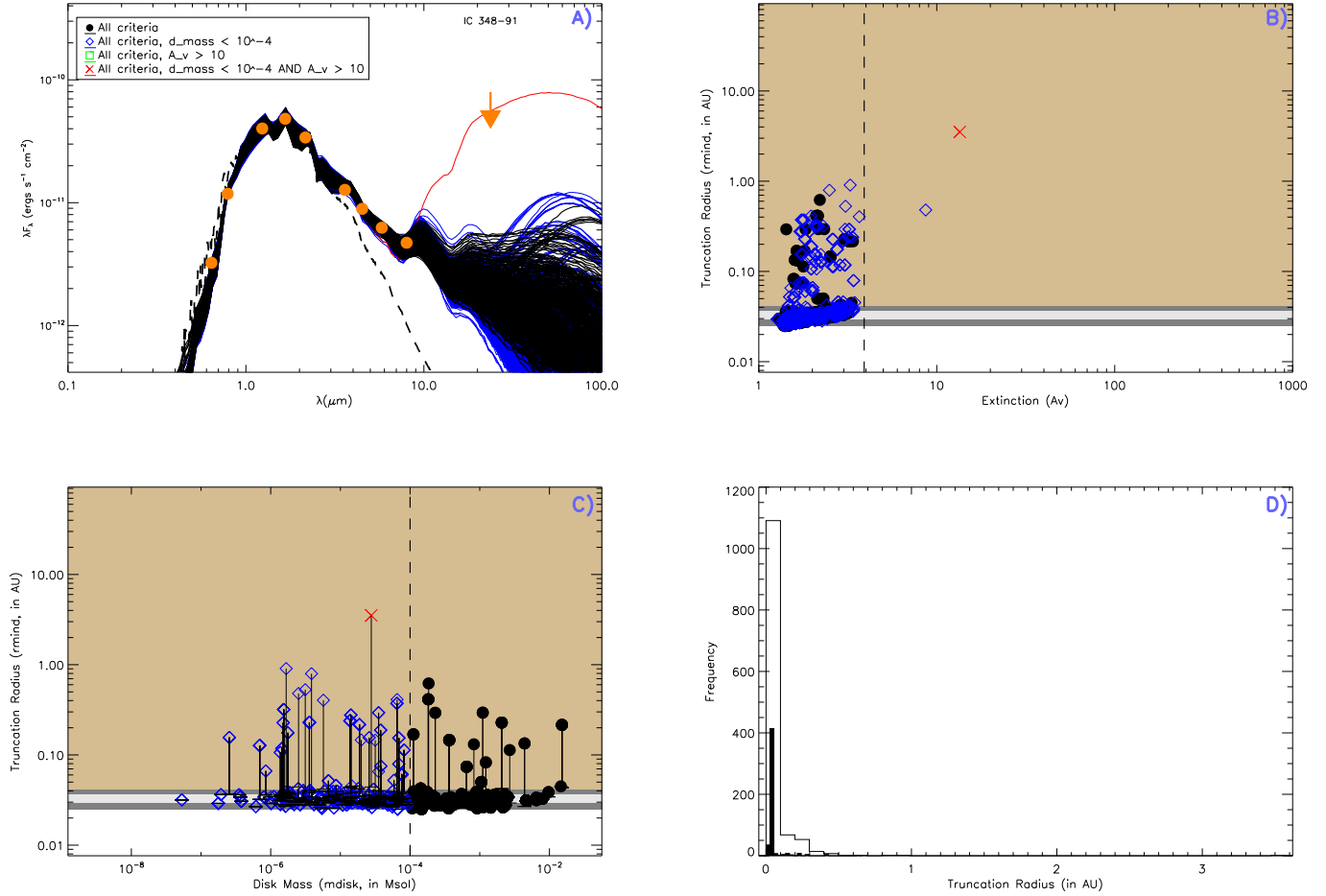


Fig. 3.— IC 348 91. This sample SED and accompanying panels represent a star for which the model grid predicts $R_{\text{trunc}} = R_{\text{co}}$. Refer to Figure 2 for further explanation of each of the above panels. Coloured plots for all sources are available in the electronic edition of the journal.

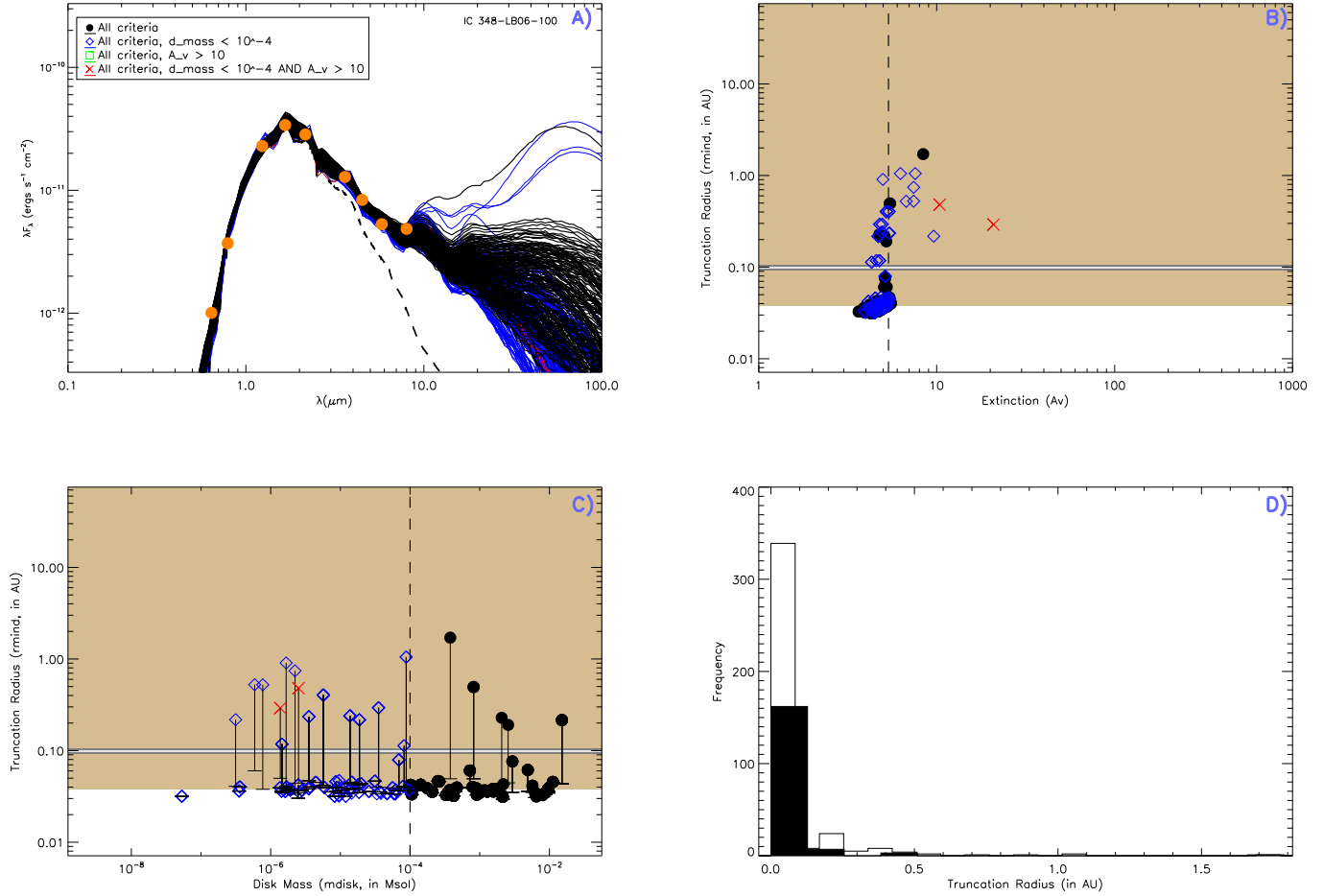


Fig. 4.— IC 348 LB06-100. This sample SED and accompanying panels represent a star for which the model grid predicts $R_{\text{trunc}} = R_{\text{sub}}$. Refer to Figure 2 for further explanation of each of the above panels. Coloured plots for all sources are available in the electronic edition of the journal.

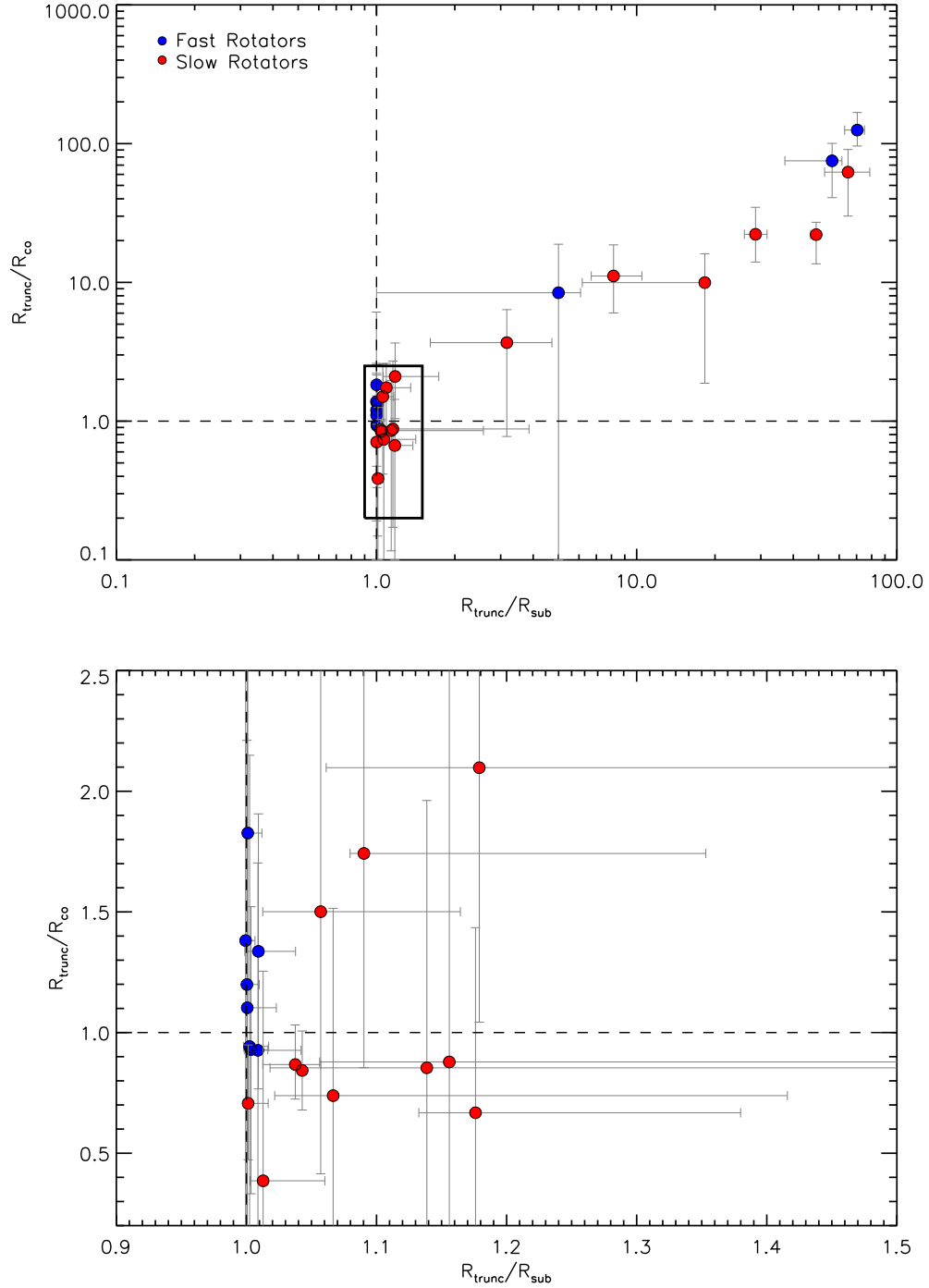


Fig. 5.— Truncation with Corotation and sublimation radii ratio plot. The plot shows the ratios of the corotation and sublimation radii in relation to the mean truncation radii for all acceptable models in the R06 grid for the entire sample (top panel). The targets within the solid box are stars with potential disks (top panel, zoomed in bottom panel), while those outside are stars that are effectively diskless. Errors in the truncation/sublimation radius ratio (x-axis) are represented as interquartile range errors, with 25% on the left and 75% on the right of each data point. Truncation/corotation radius ratio errors are represented as 1σ . See electronic edition of the journal for a coloured version of this figure.

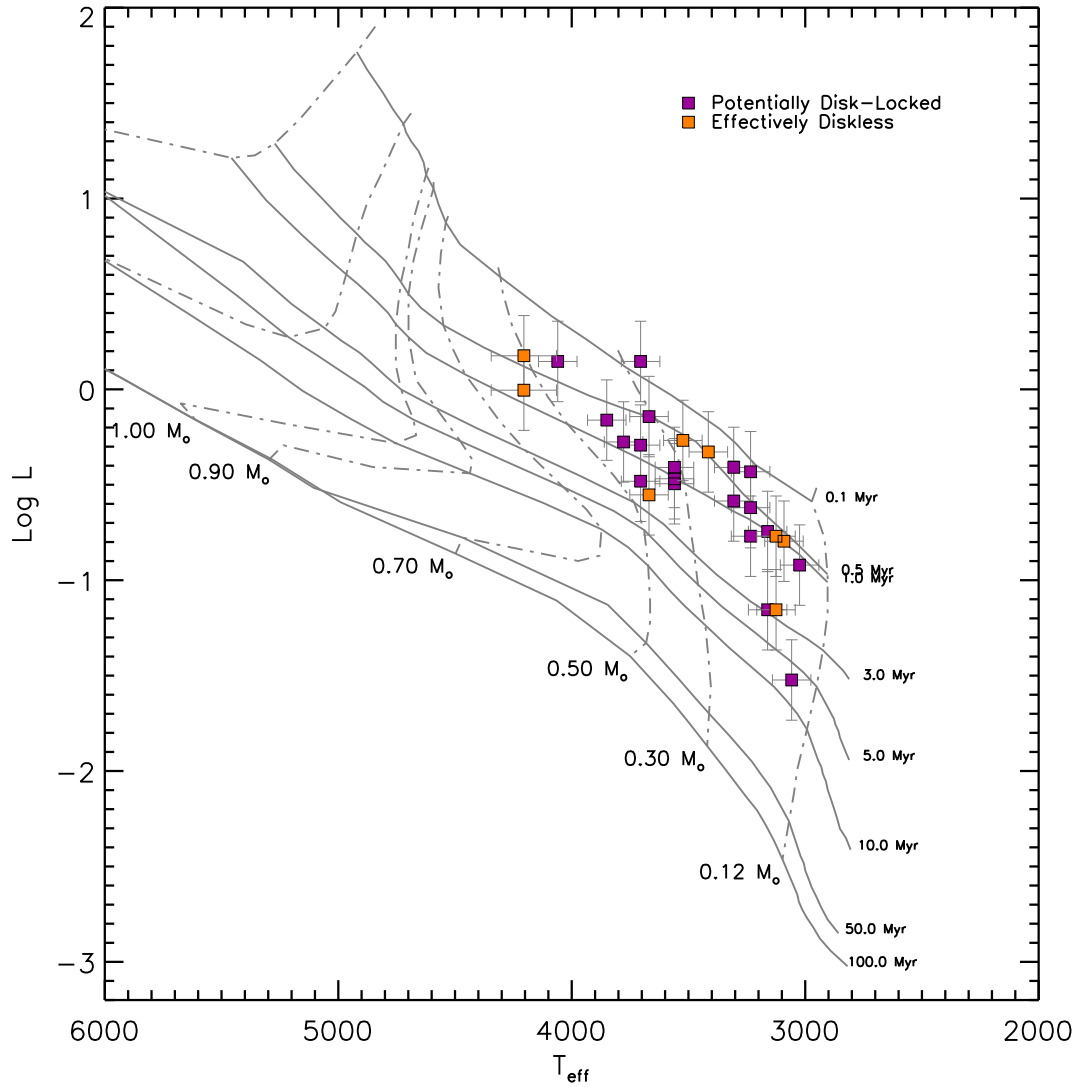


Fig. 6.— HR Diagram with over plotted tracks and isochrones using DM97. All errors represented in both log L & log T are 1σ . See electronic edition of the journal for a coloured version of this figure.

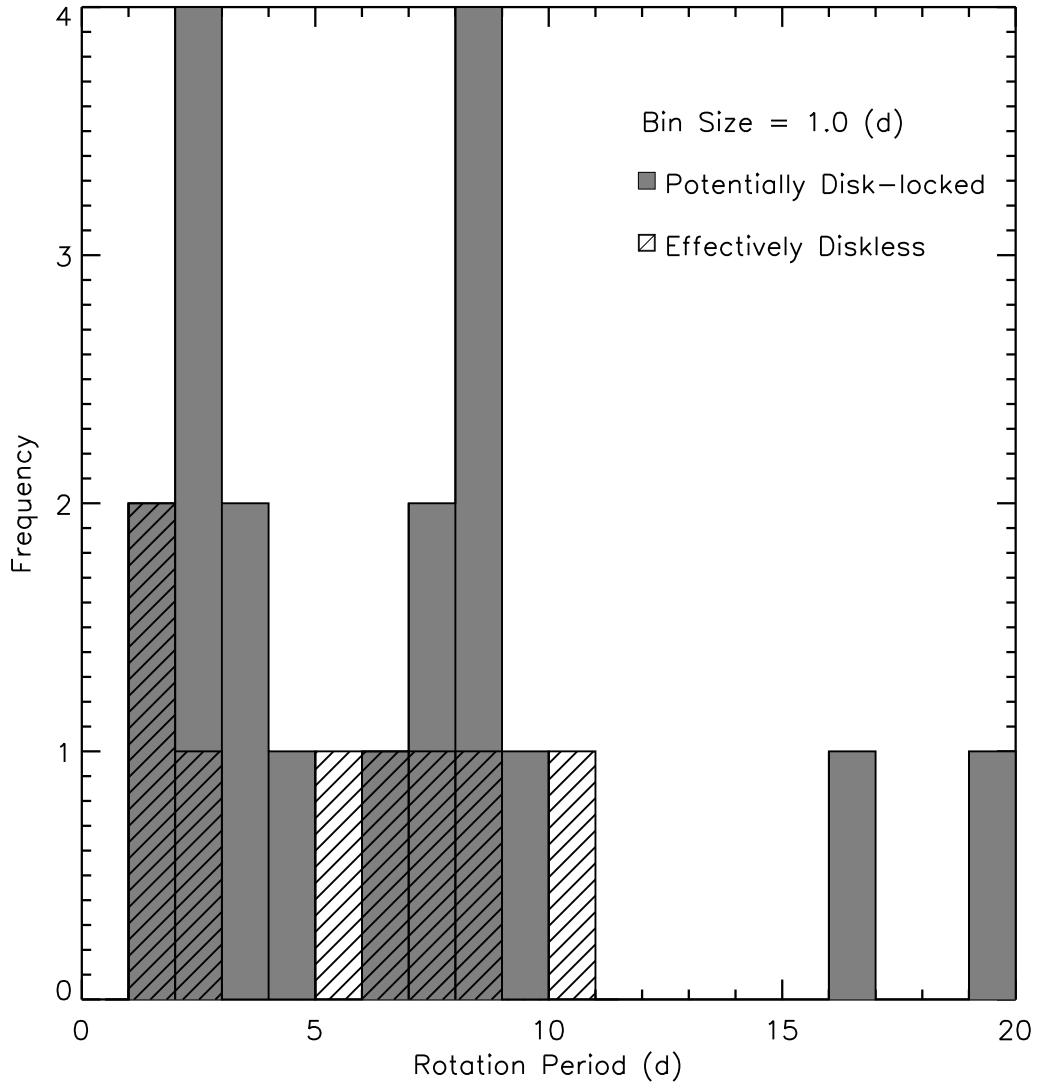


Fig. 7.— Rotation period histogram of potentially disk-locked (gray) and effectively diskless stars (empty hatched). Though the potentially disk-locked stars are greater in number than the effectively diskless stars, this histogram supports the null hypothesis that both distributions are from the same parent distribution.

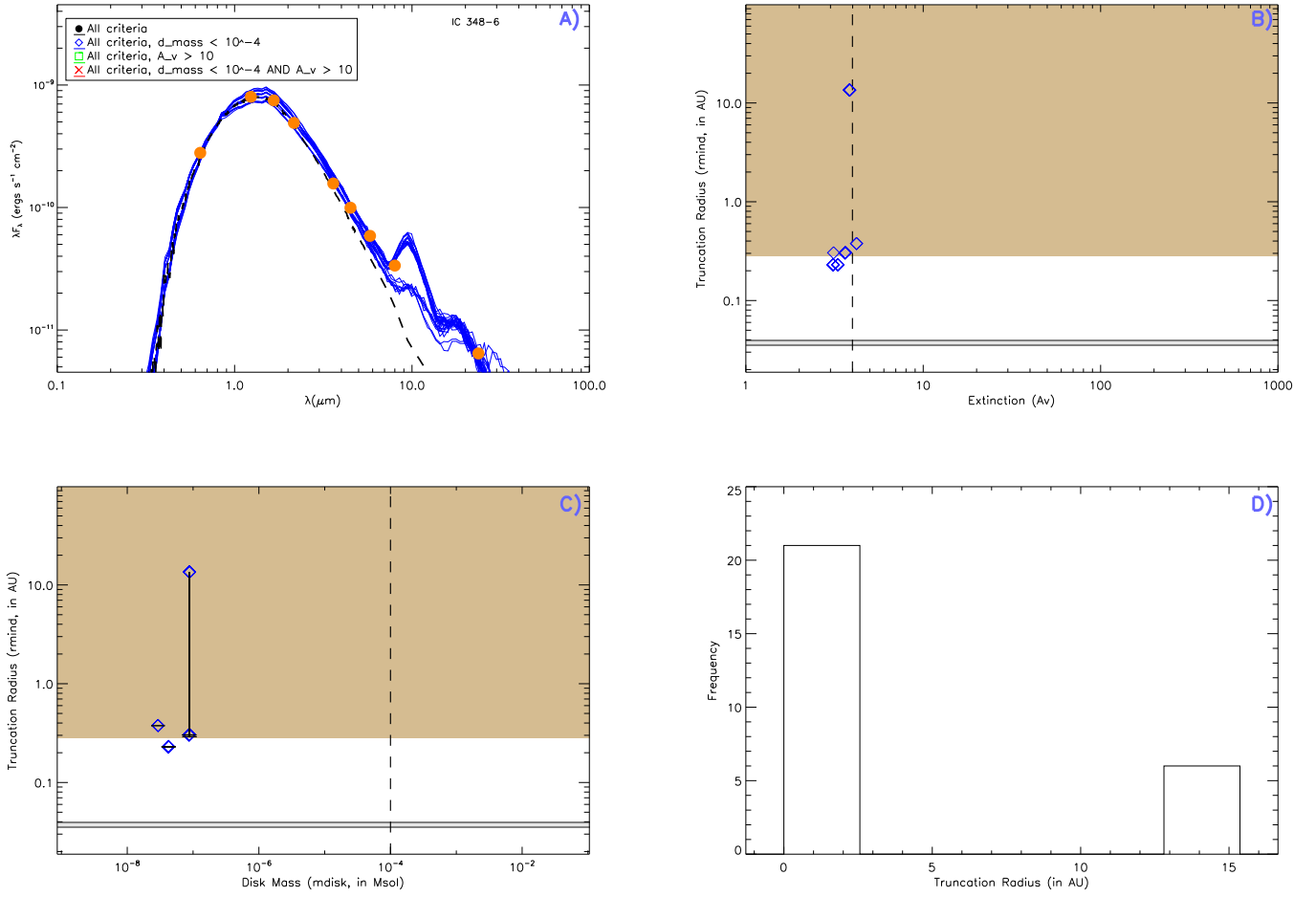


Fig. 8.— IC 348 6. Refer to Figure 2 for further explanation of each of the above panels. Figures 7 - 37 are available in the online version of the Journal.

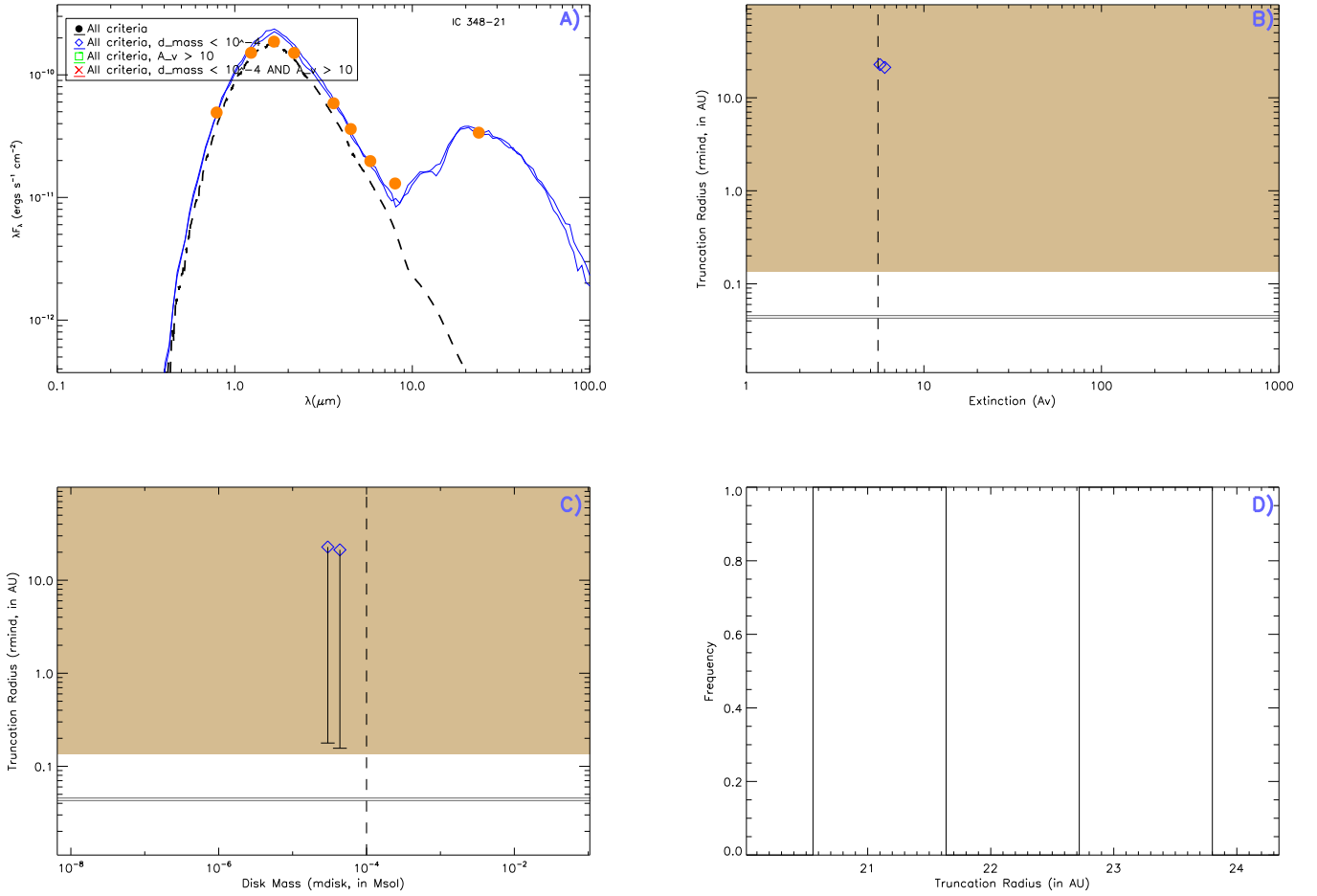


Fig. 9.— IC 348 21. Refer to Figure 2 for further explanation of each of the above panels. Figures 7 - 37 are available in the online version of the Journal.

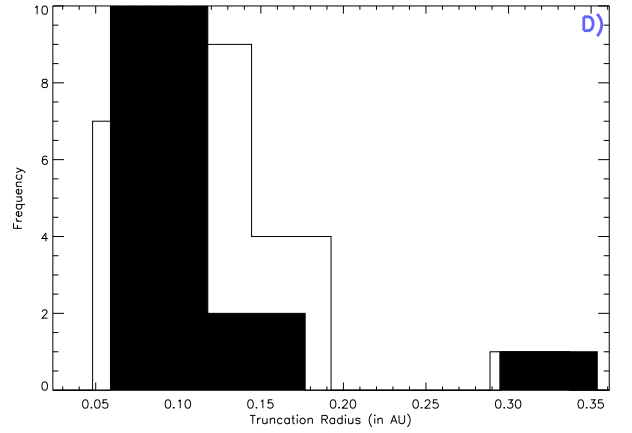
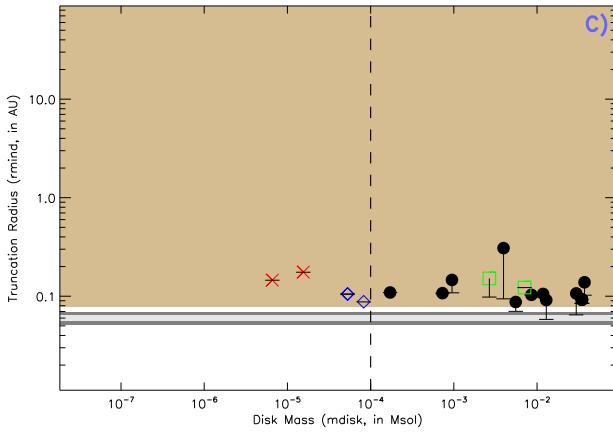
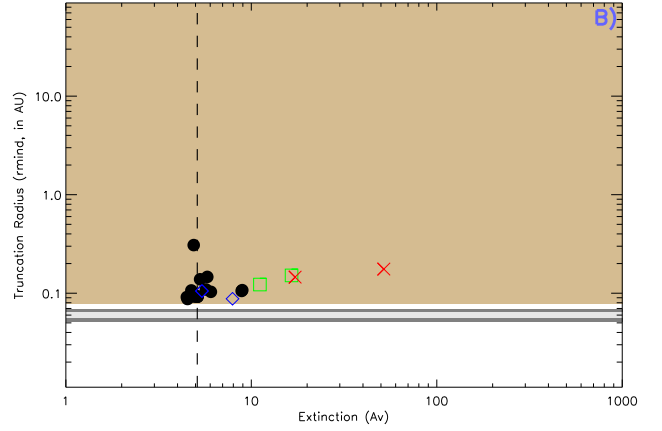
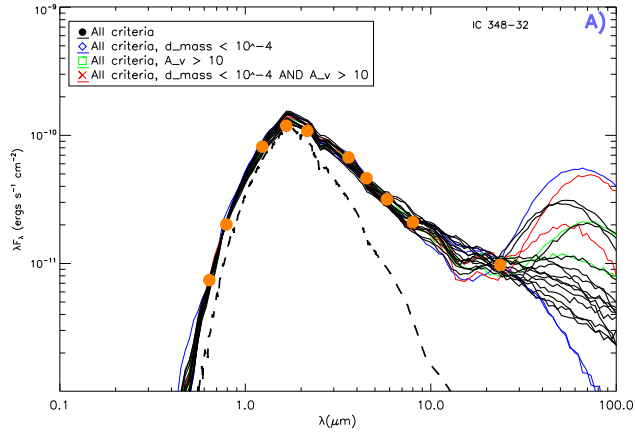


Fig. 10.— IC 348 32. Refer to Figure 2 for further explanation of each of the above panels. Figures 7 - 37 are available in the online version of the Journal.

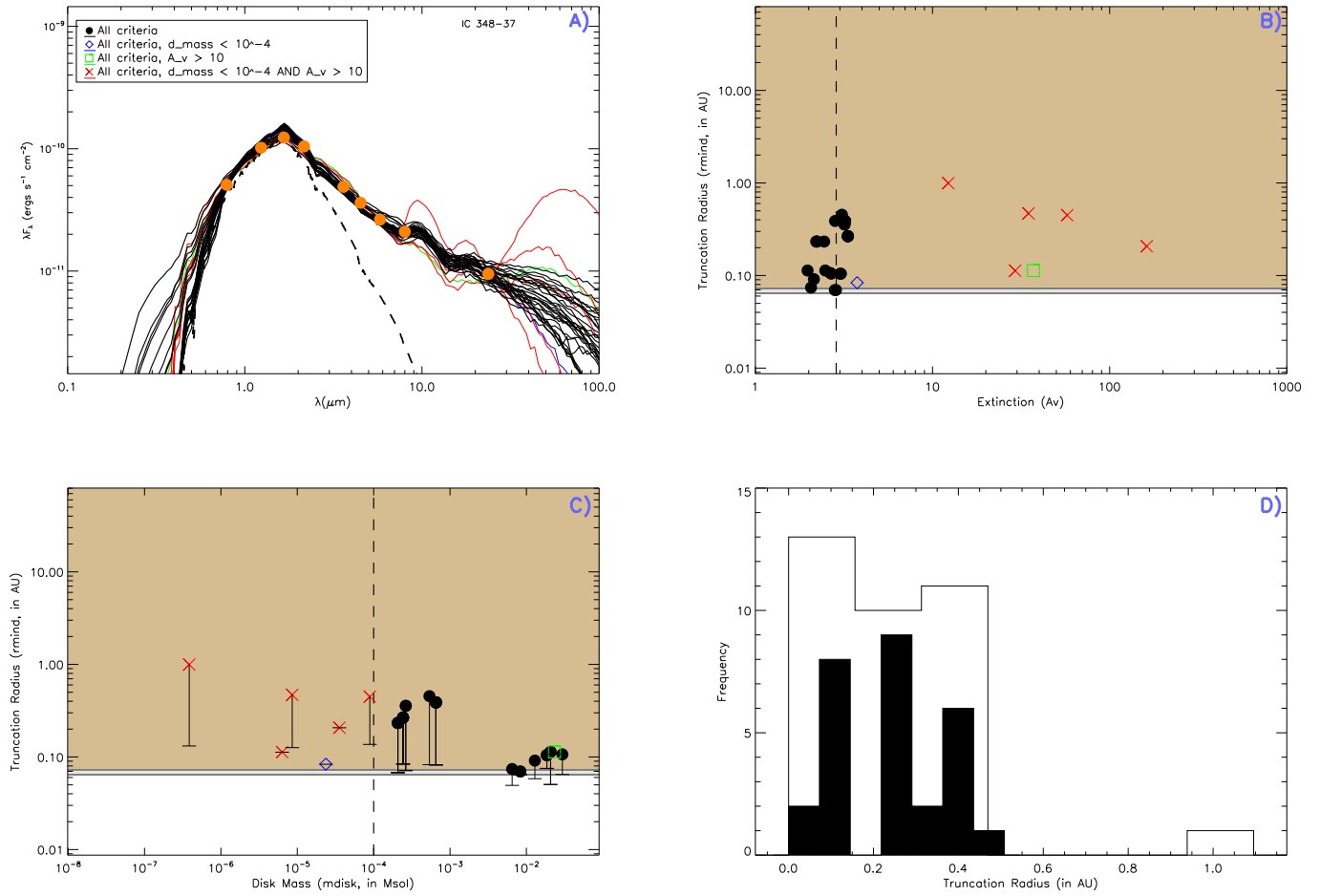


Fig. 11.— IC 348 37. Refer to Figure 2 for further explanation of each of the above panels. Figures 7 - 37 are available in the online version of the Journal.

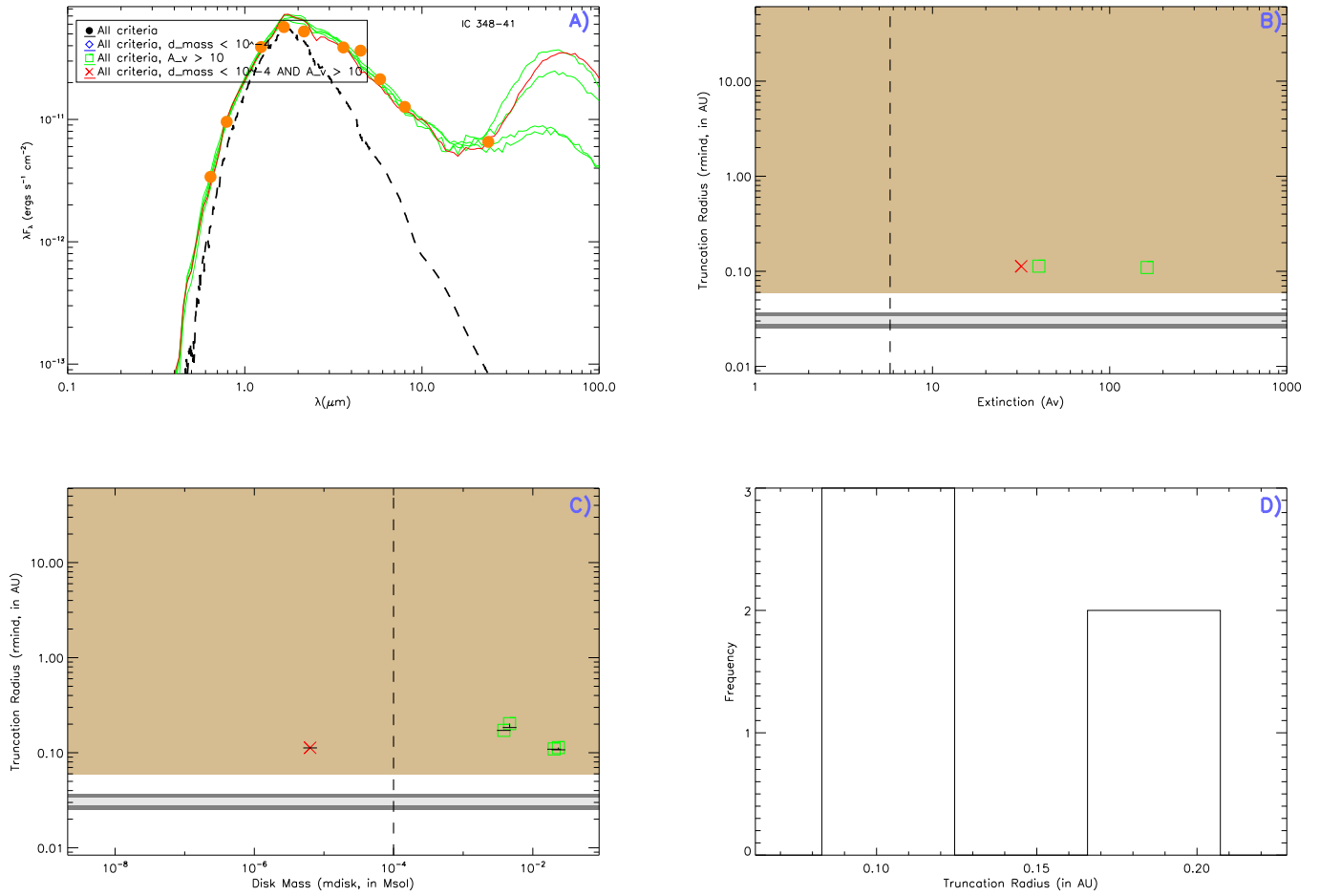


Fig. 12.— IC 348 41. Refer to Figure 2 for further explanation of each of the above panels. Figures 7 - 37 are available in the online version of the Journal.

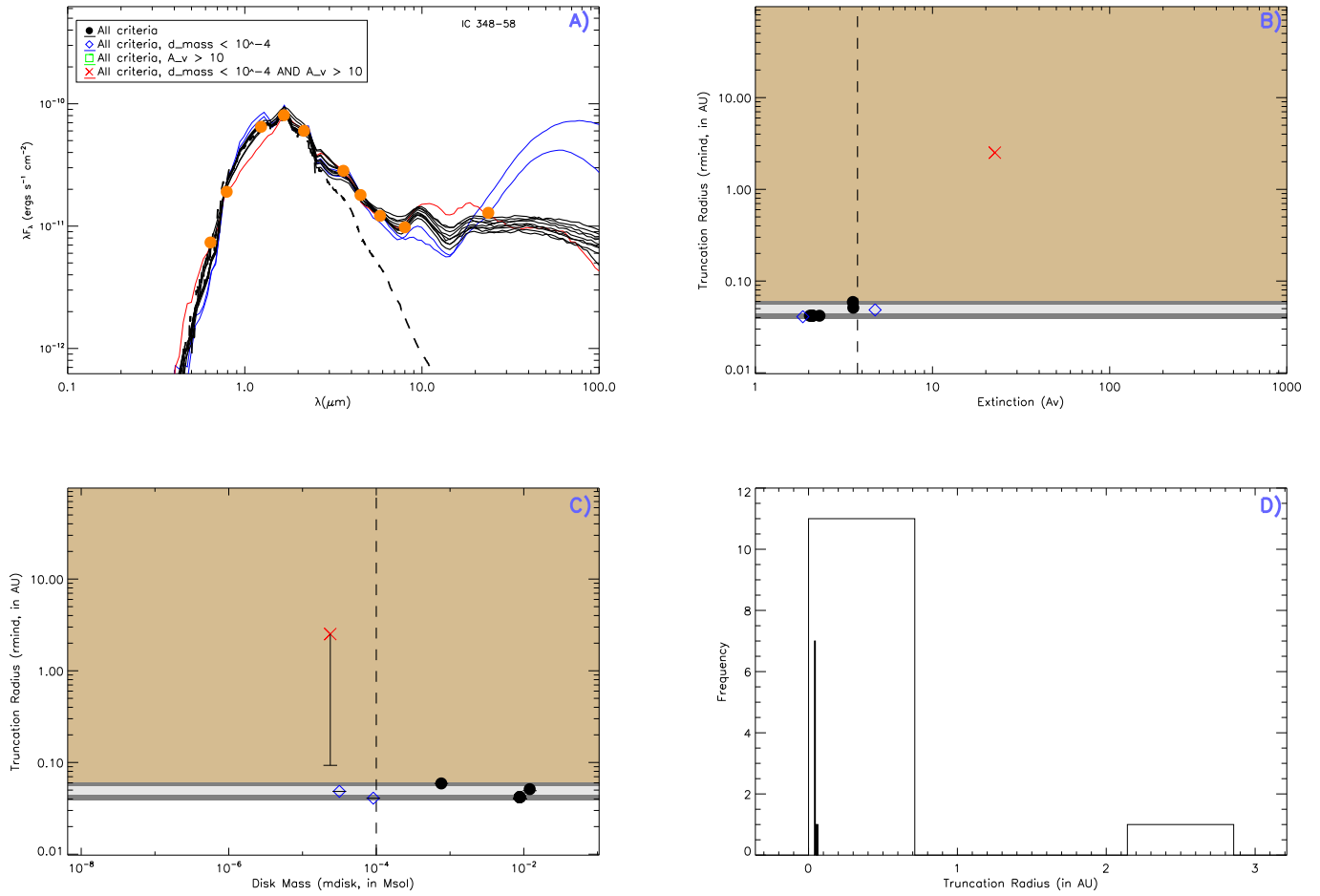


Fig. 13.— IC 348 58. Refer to Figure 2 for further explanation of each of the above panels. Figures 7 - 37 are available in the online version of the Journal.

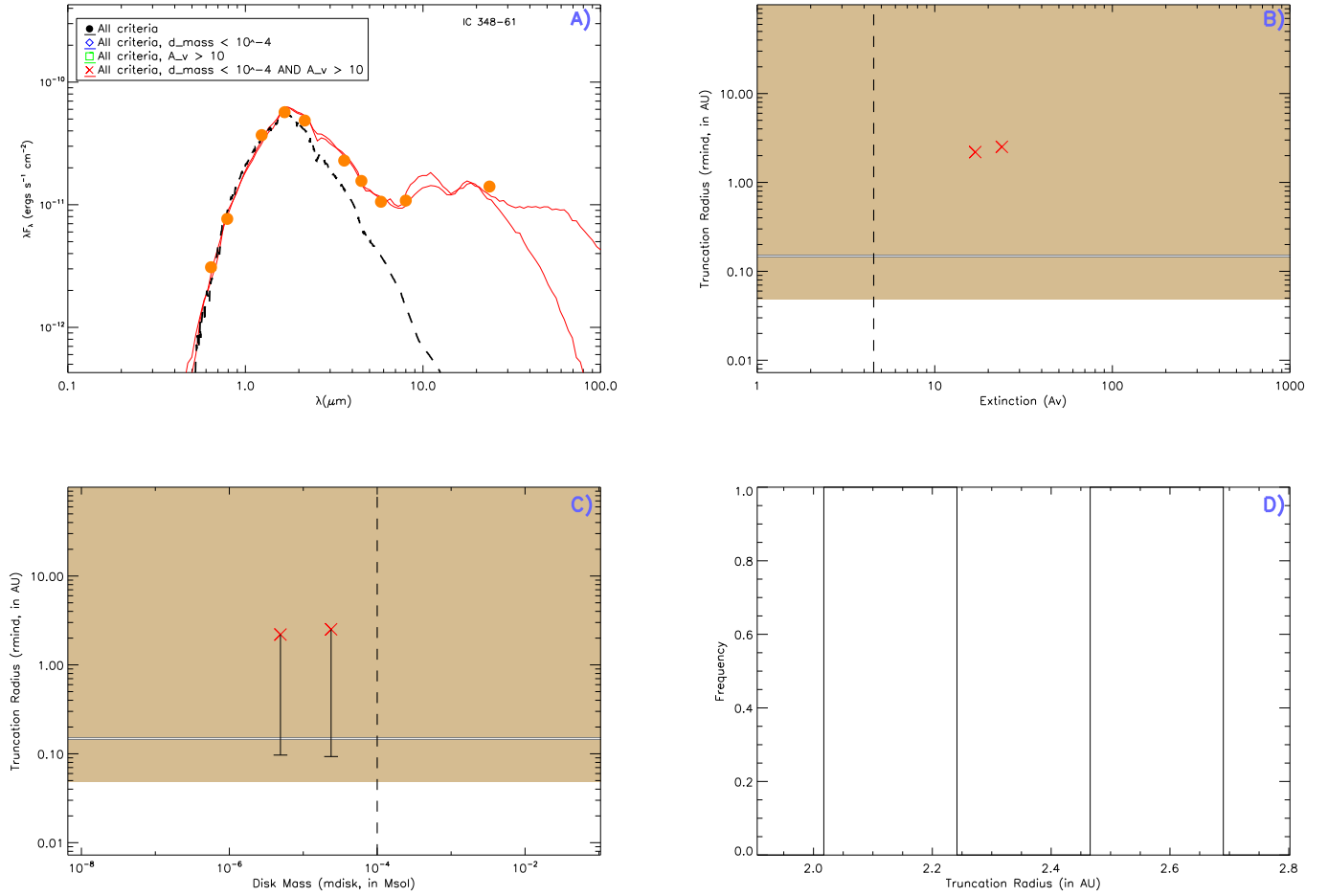


Fig. 14.— IC 348 61. Refer to Figure 2 for further explanation of each of the above panels. Figures 7 - 37 are available in the online version of the Journal.

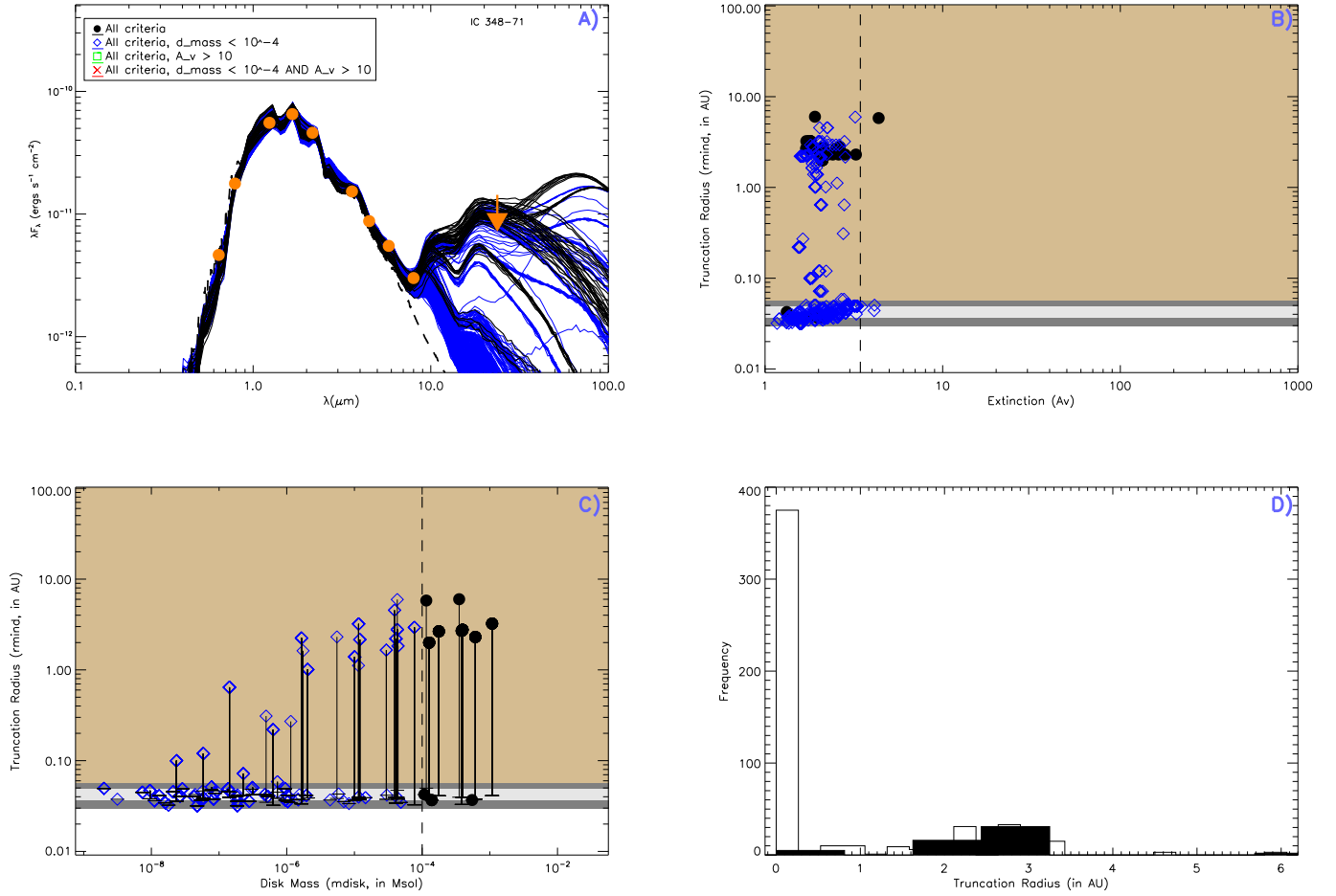


Fig. 15.— IC 348 71. Refer to Figure 2 for further explanation of each of the above panels. Figures 7 - 37 are available in the online version of the Journal.

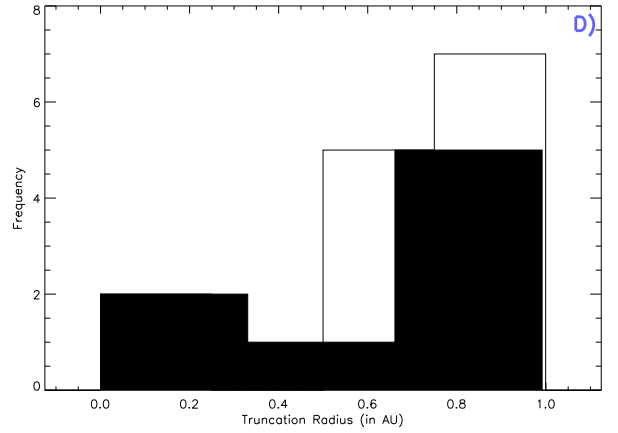
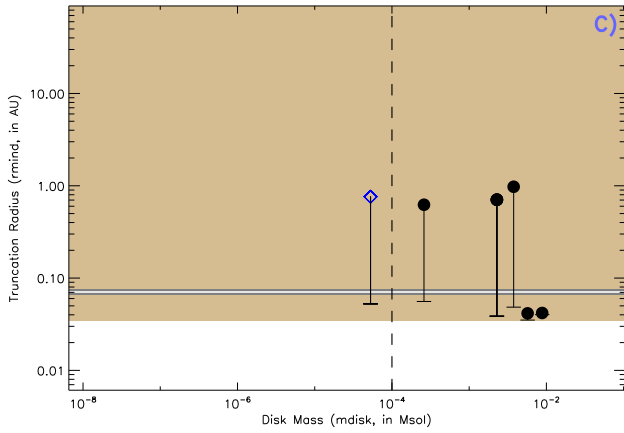
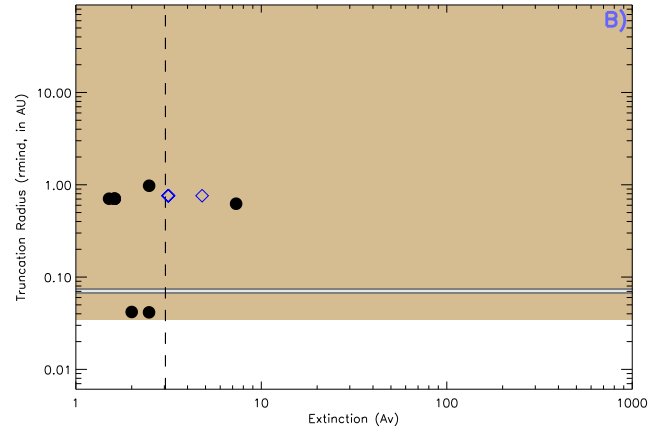
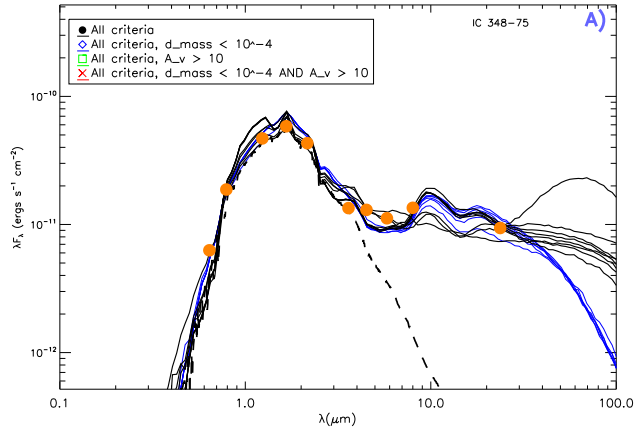


Fig. 16.— IC 348 75. Refer to Figure 2 for further explanation of each of the above panels. Figures 7 - 37 are available in the online version of the Journal.

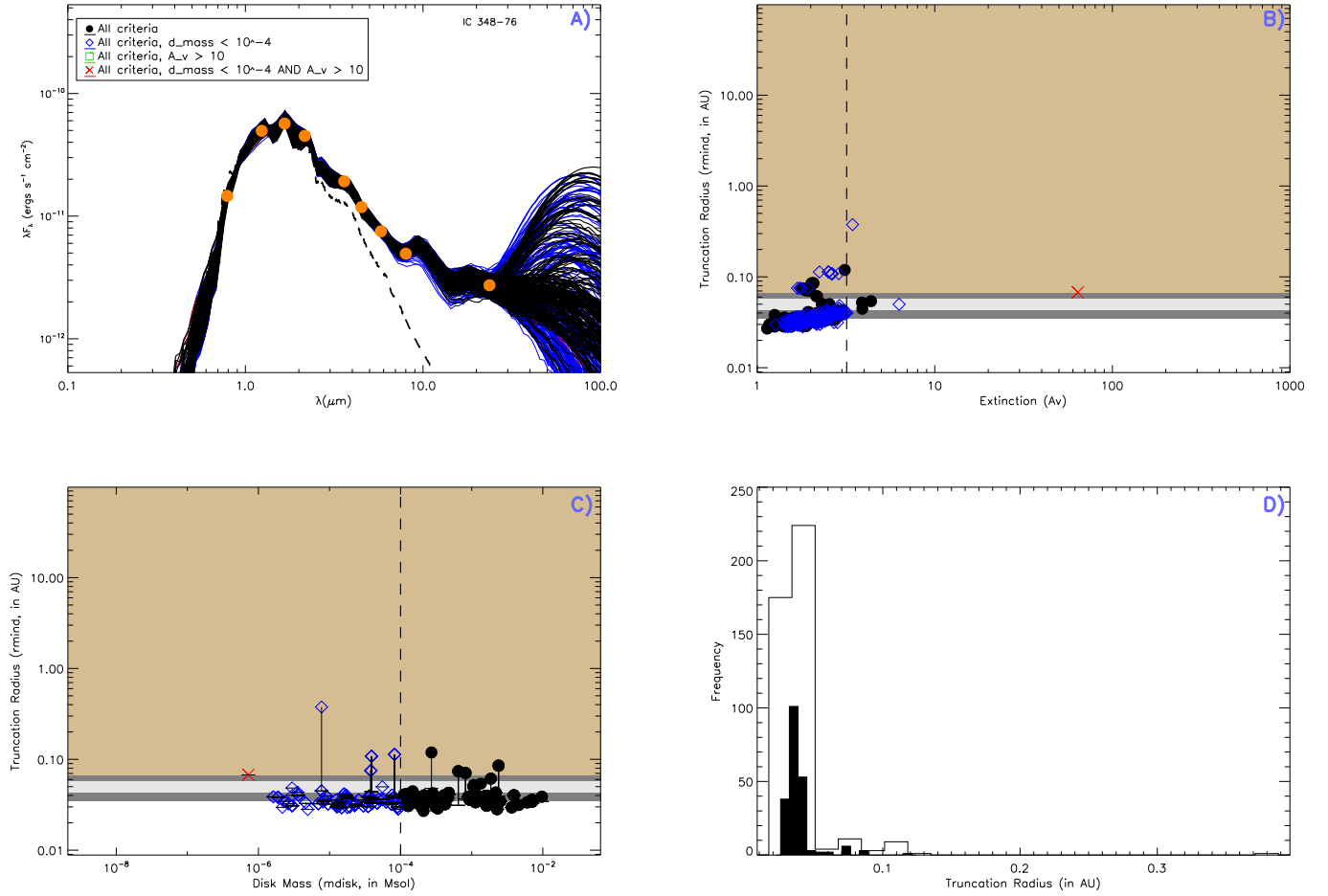


Fig. 17.— IC 348 76. Refer to Figure 2 for further explanation of each of the above panels. Figures 7 - 37 are available in the online version of the Journal.

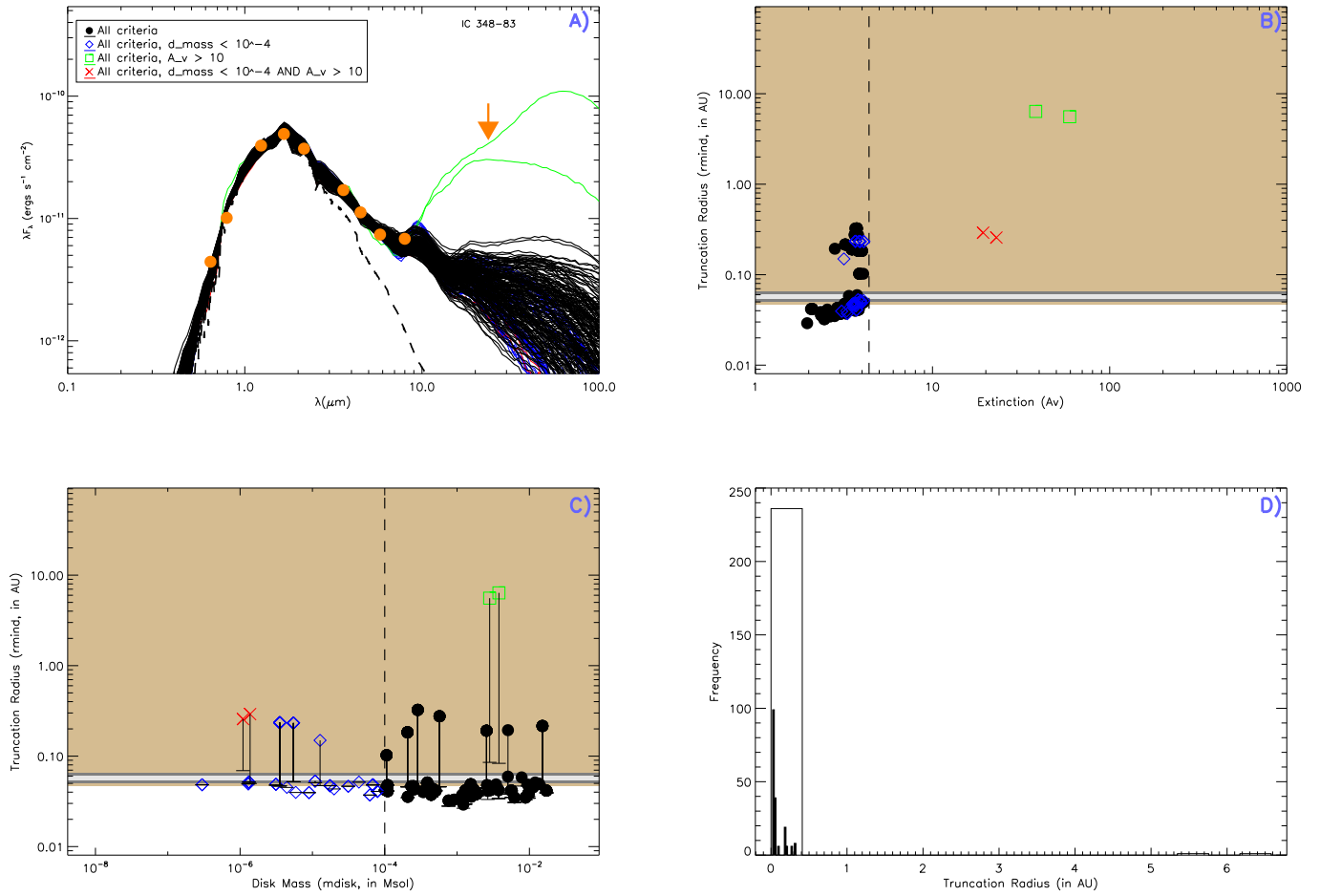


Fig. 18.— IC 348 83. Refer to Figure 2 for further explanation of each of the above panels. Figures 7 - 37 are available in the online version of the Journal.

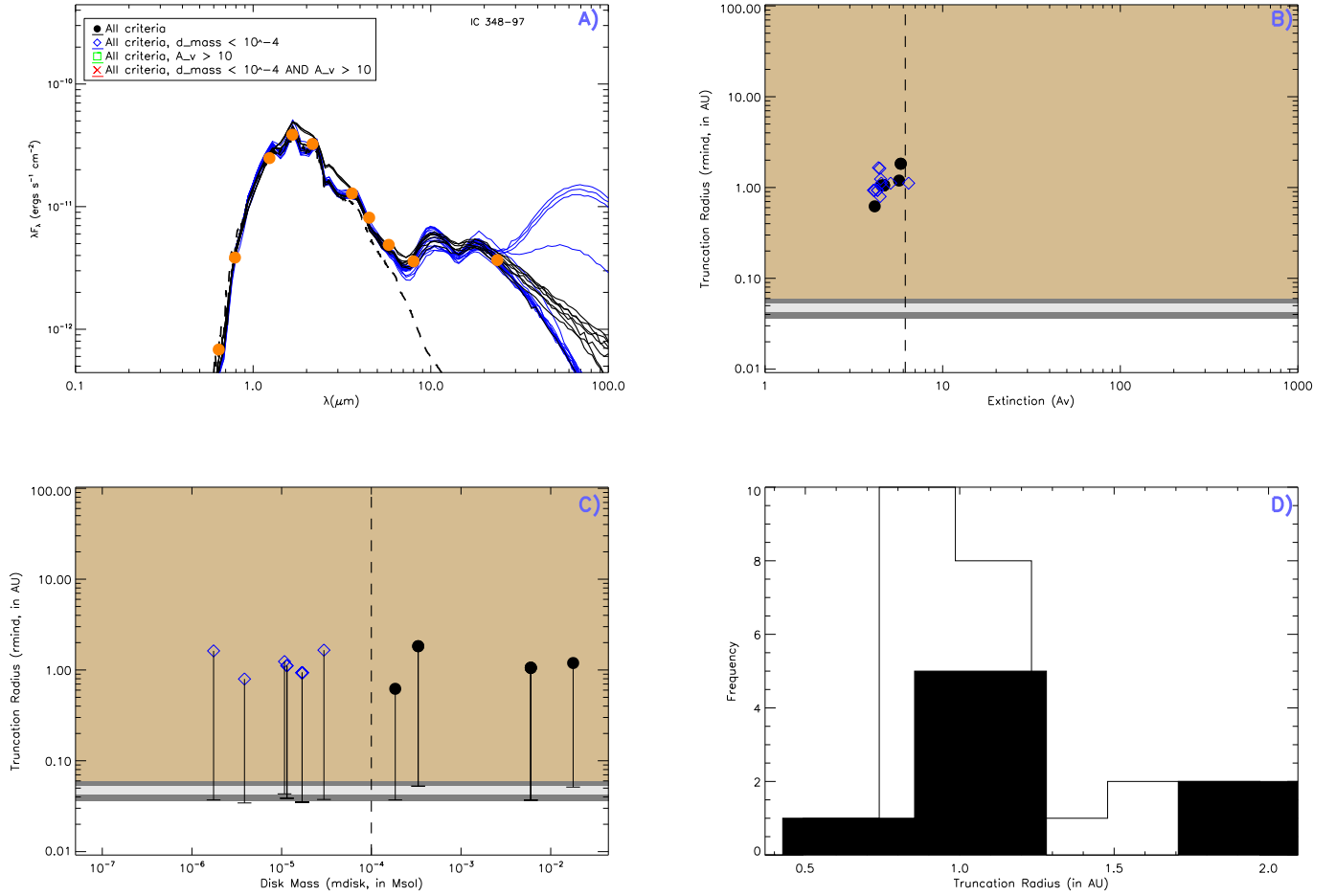


Fig. 19.— IC 348 97. Refer to Figure 2 for further explanation of each of the above panels. Figures 7 - 37 are available in the online version of the Journal.

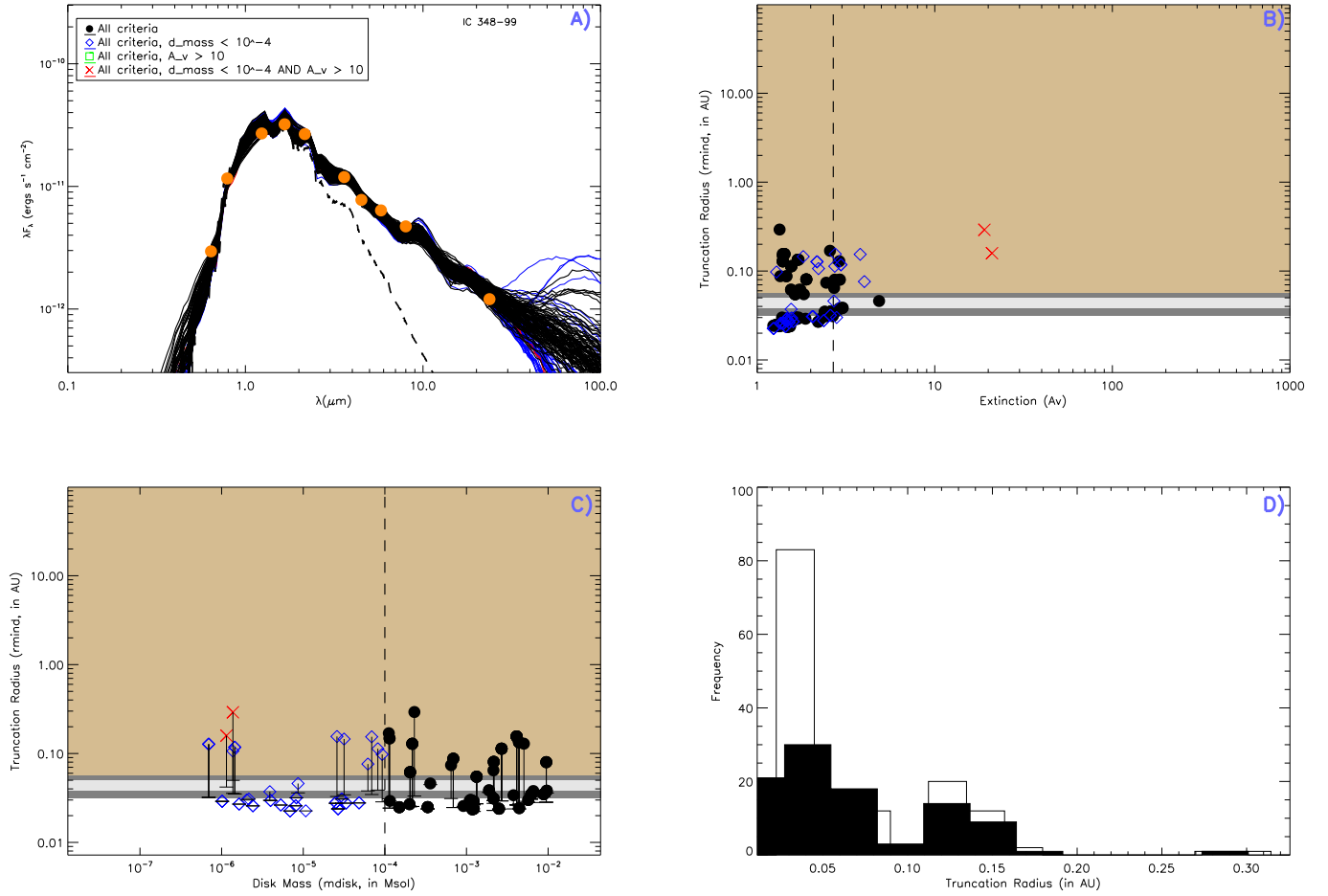


Fig. 20.— IC 348 99. Refer to Figure 2 for further explanation of each of the above panels. Figures 7 - 37 are available in the online version of the Journal.

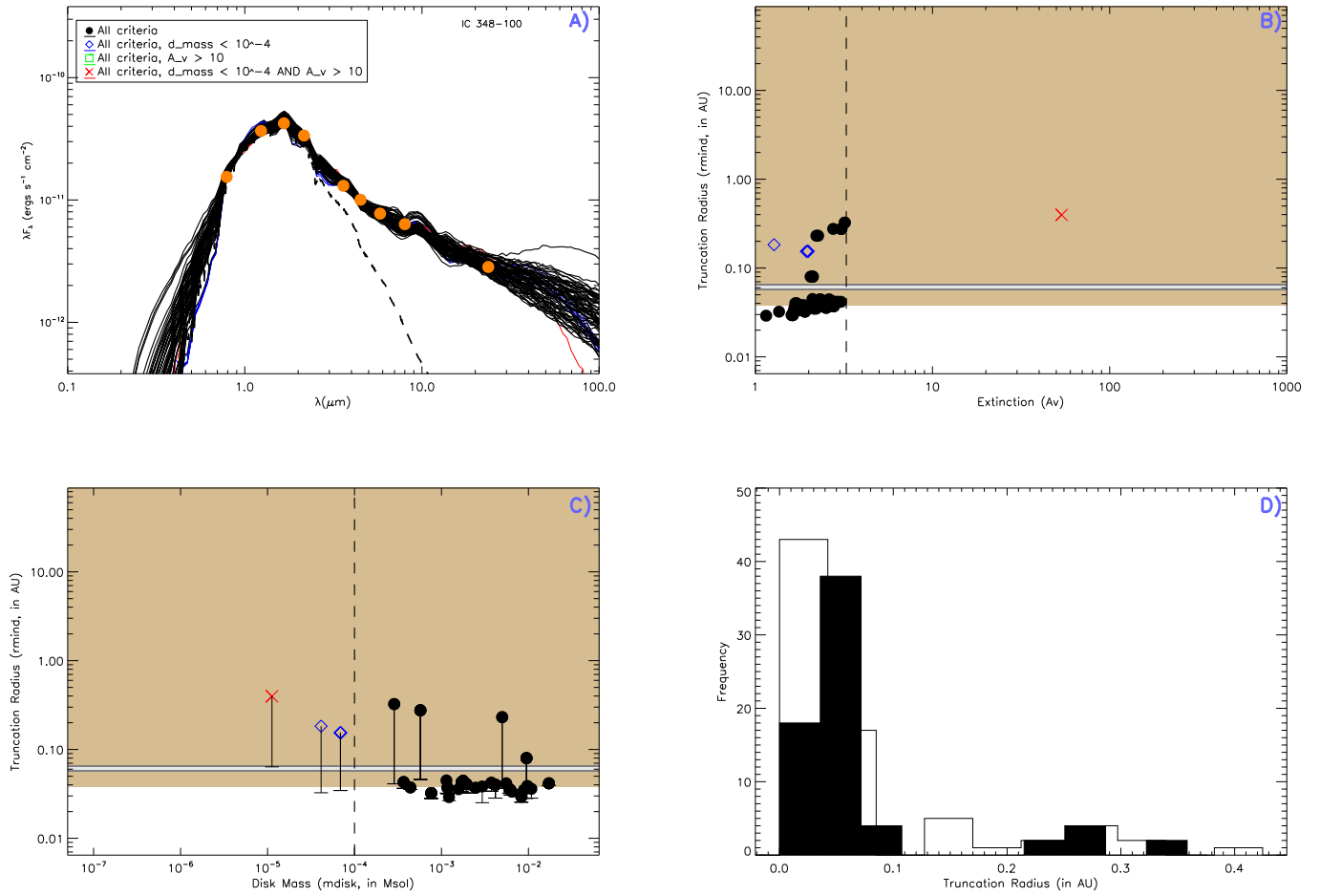


Fig. 21.— IC 348 100. Refer to Figure 2 for further explanation of each of the above panels. Figures 7 - 37 are available in the online version of the Journal.

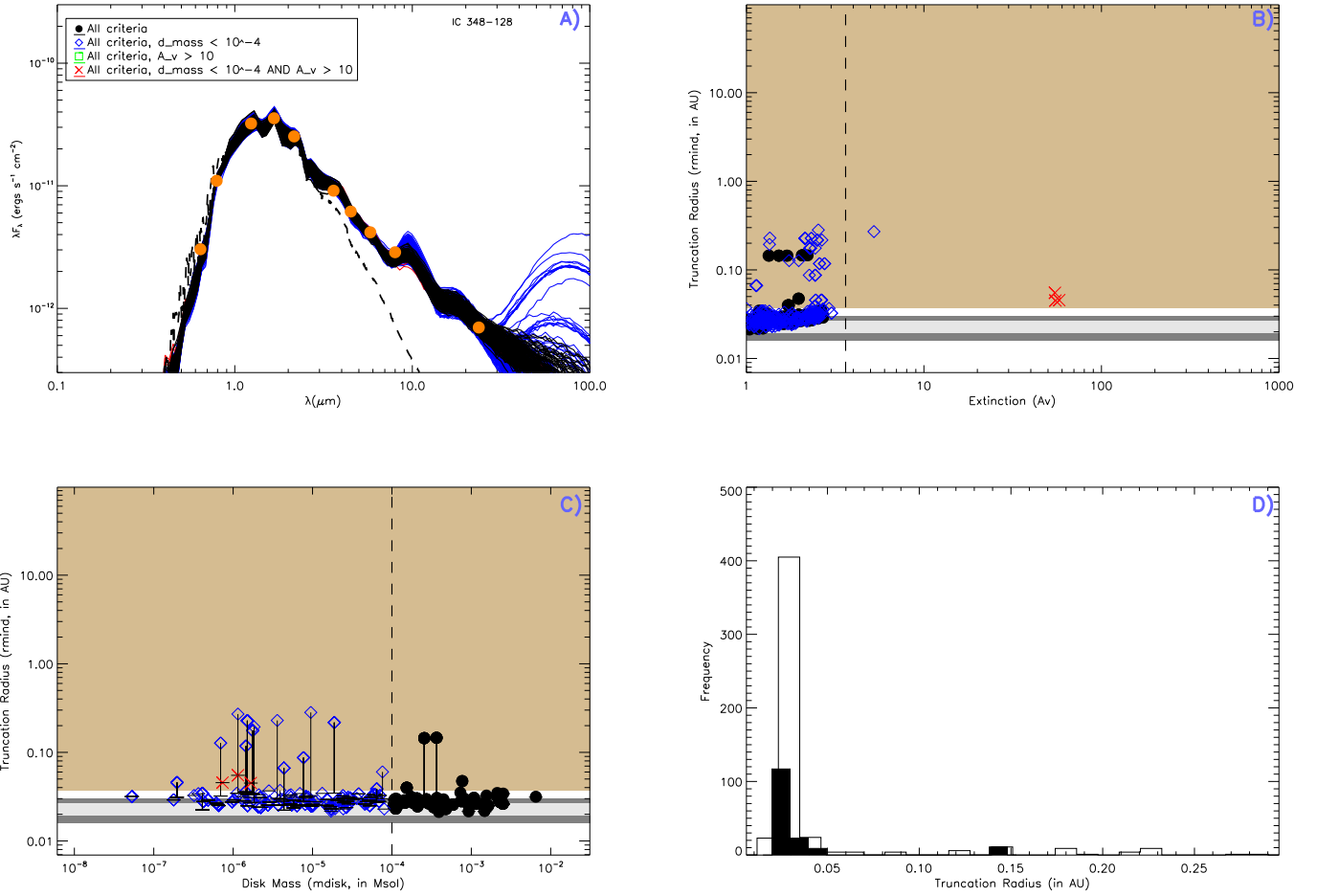


Fig. 22.— IC 348 128. Refer to Figure 2 for further explanation of each of the above panels. Figures 7 - 37 are available in the online version of the Journal.

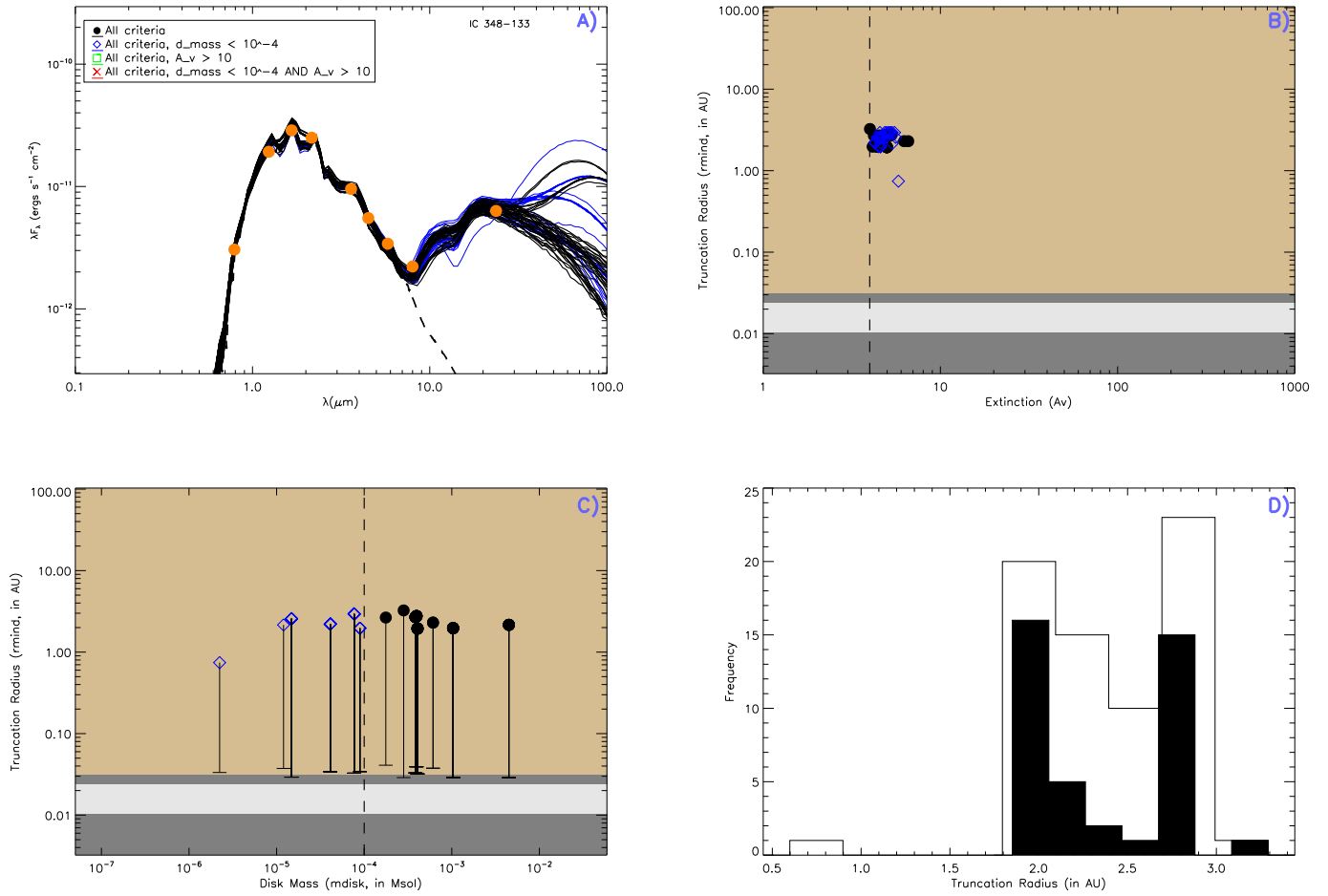


Fig. 23.— IC 348 133. Refer to Figure 2 for further explanation of each of the above panels. Figures 7 - 37 are available in the online version of the Journal.

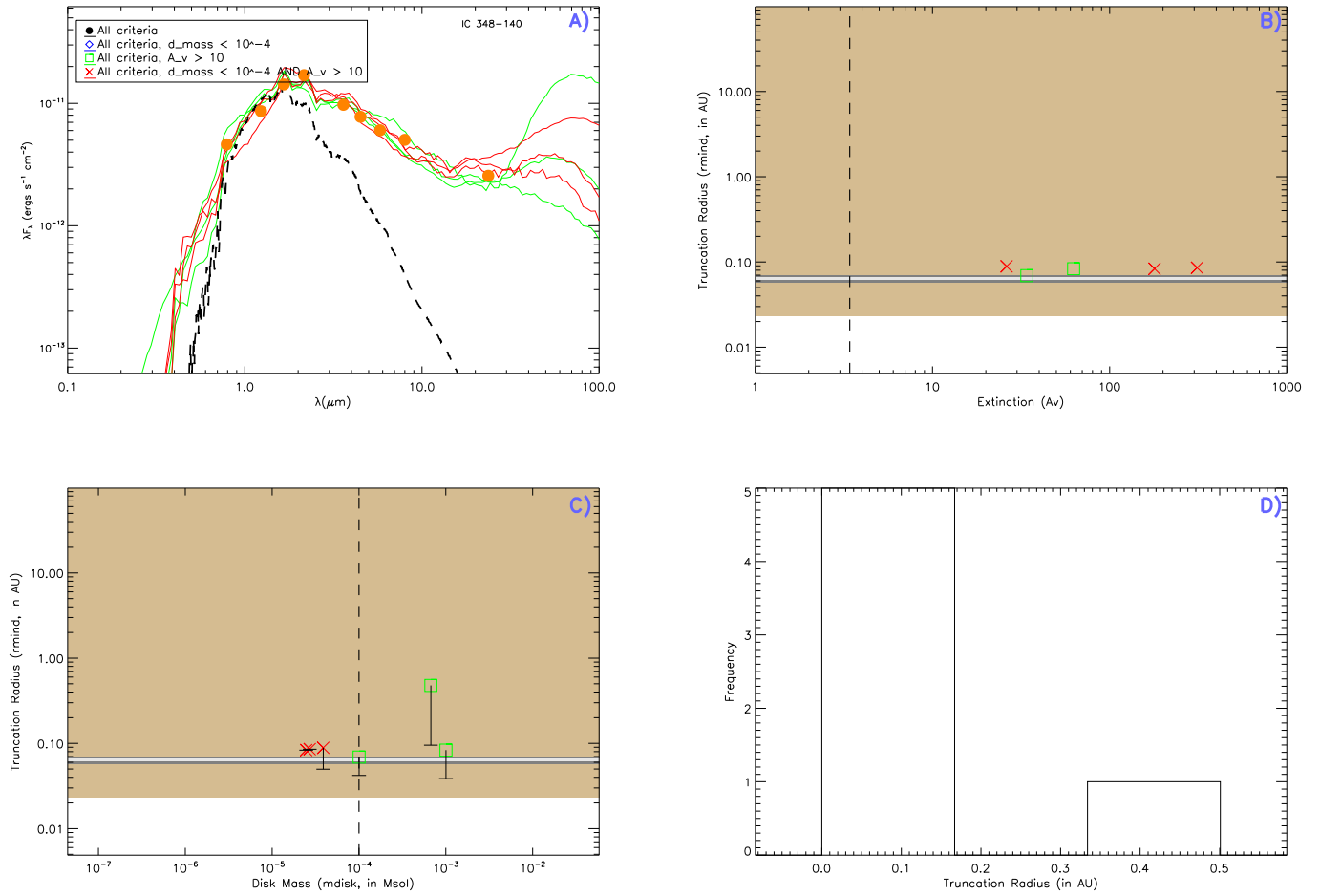


Fig. 24.— IC 348 140. Refer to Figure 2 for further explanation of each of the above panels. Figures 7 - 37 are available in the online version of the Journal.

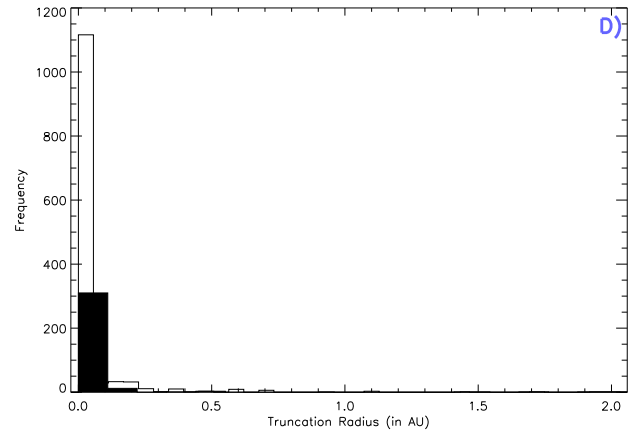
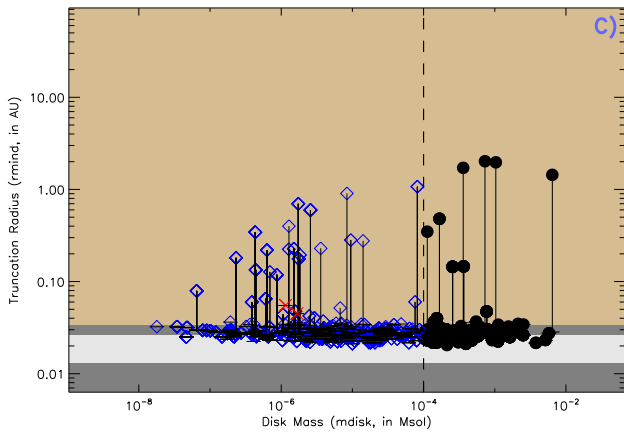
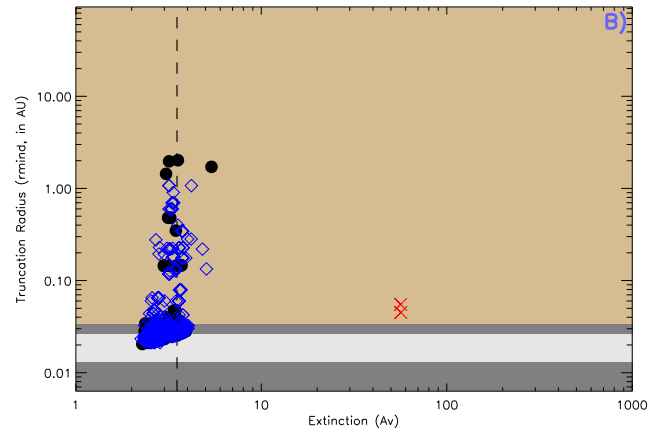
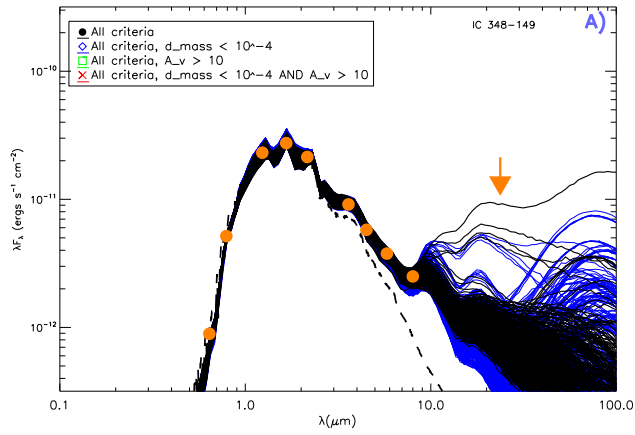


Fig. 25.— IC 348 149. Refer to Figure 2 for further explanation of each of the above panels. Figures 7 - 37 are available in the online version of the Journal.

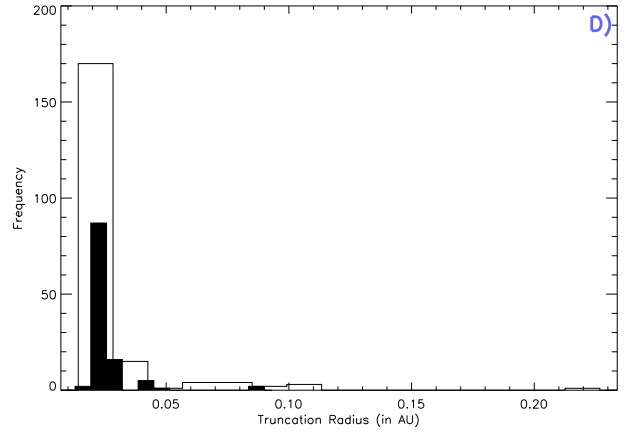
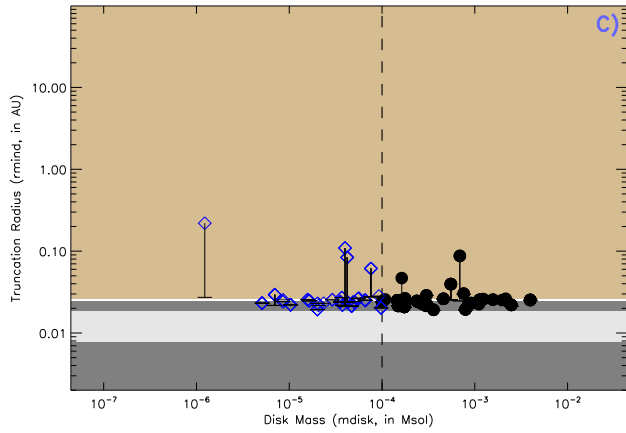
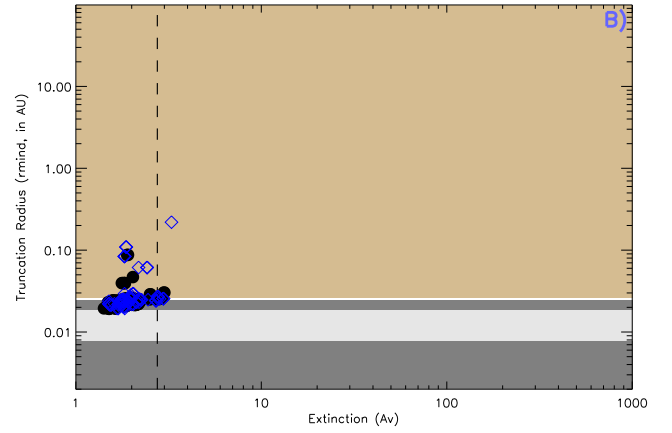
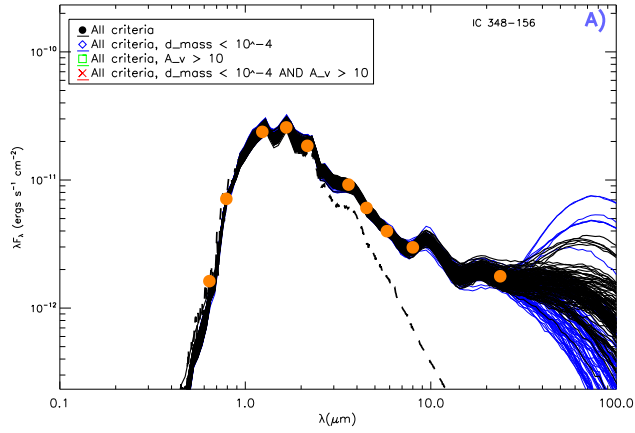


Fig. 26.— IC 348 156. Refer to Figure 2 for further explanation of each of the above panels. Figures 7 - 37 are available in the online version of the Journal.

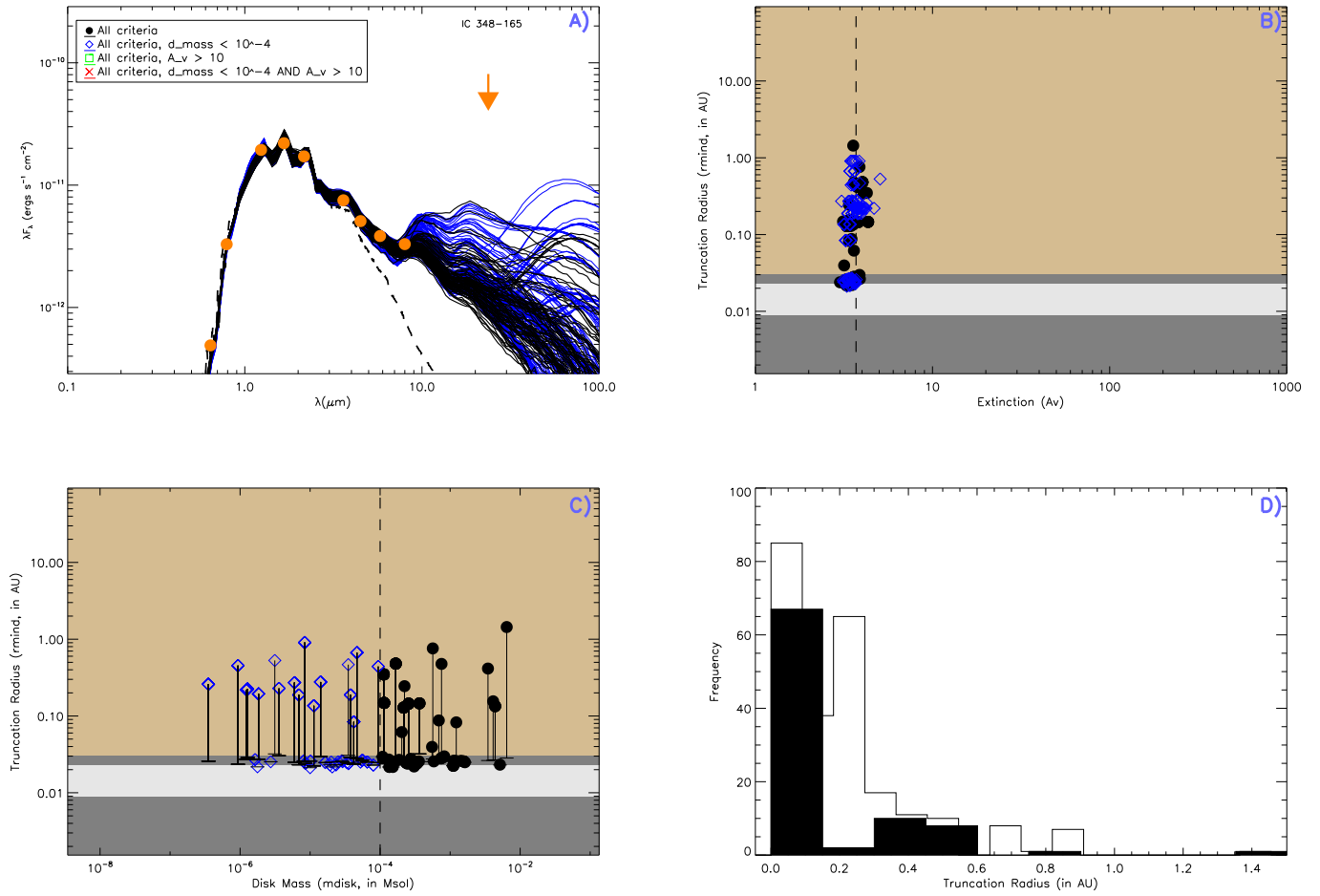


Fig. 27.— IC 348 165. Refer to Figure 2 for further explanation of each of the above panels. Figures 7 - 37 are available in the online version of the Journal.

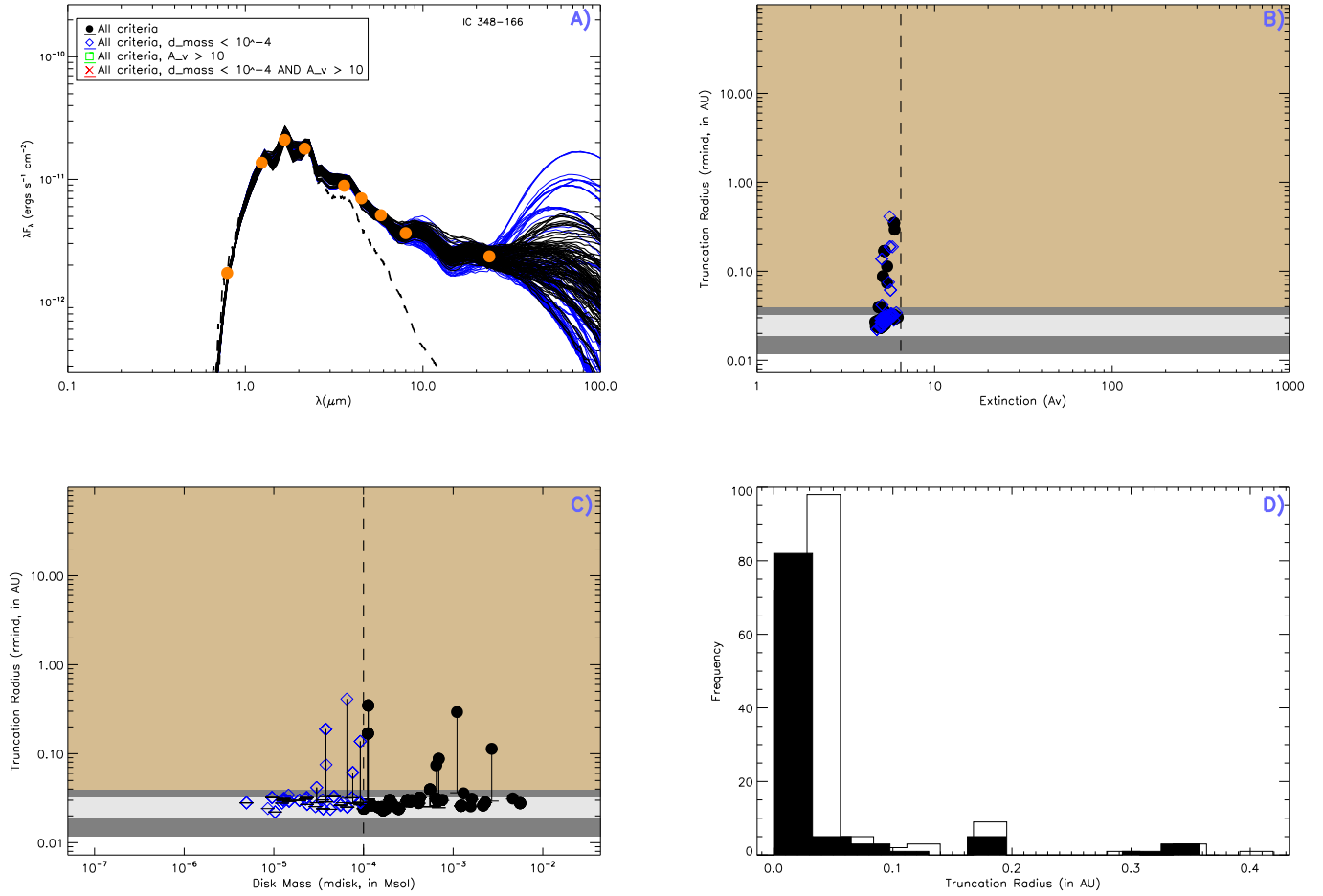


Fig. 28.— IC 348 166. Refer to Figure 2 for further explanation of each of the above panels. Figures 7 - 37 are available in the online version of the Journal.

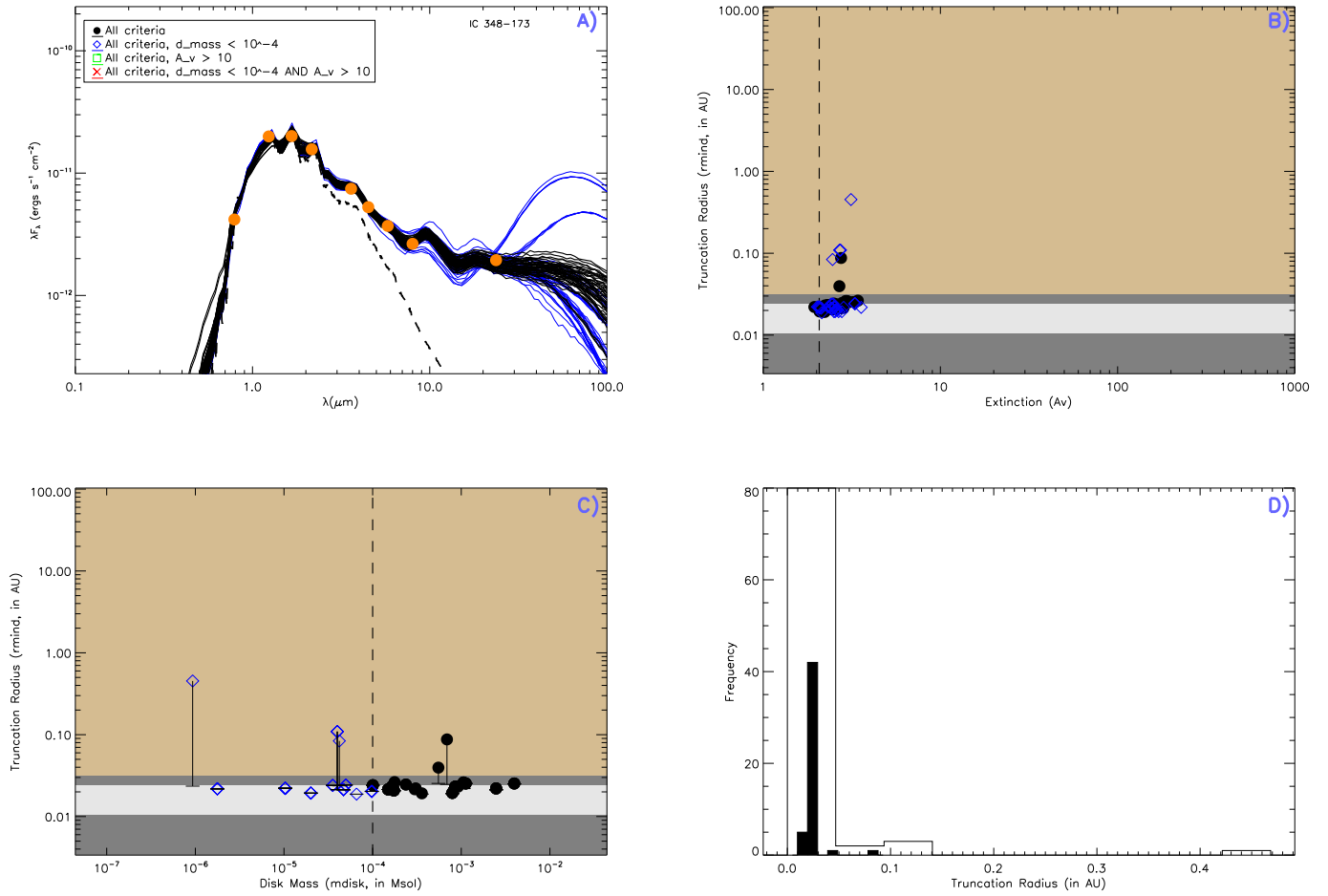


Fig. 29.— IC 348 173. Refer to Figure 2 for further explanation of each of the above panels. Figures 7 - 37 are available in the online version of the Journal.

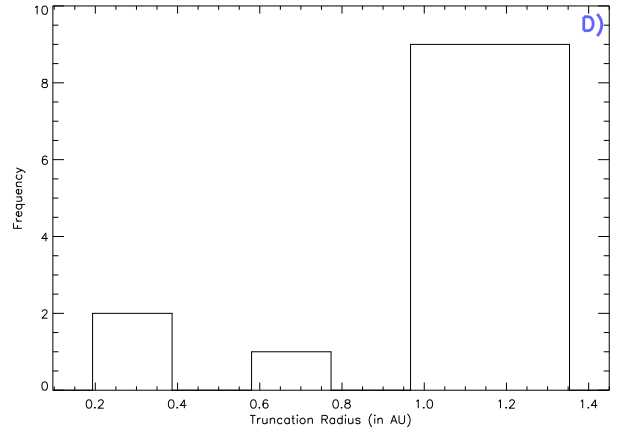
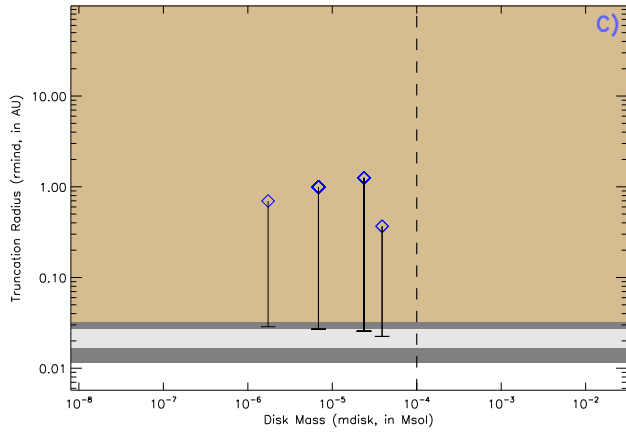
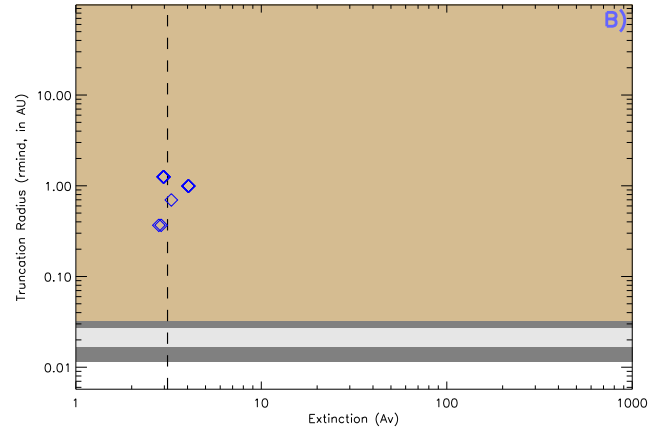
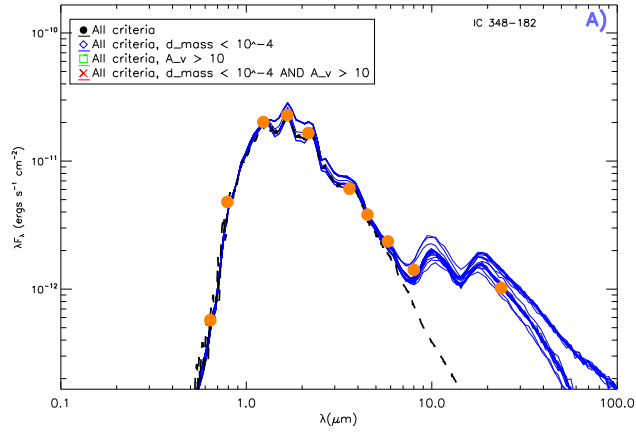


Fig. 30.— IC 348 182. Refer to Figure 2 for further explanation of each of the above panels. Figures 7 - 37 are available in the online version of the Journal.

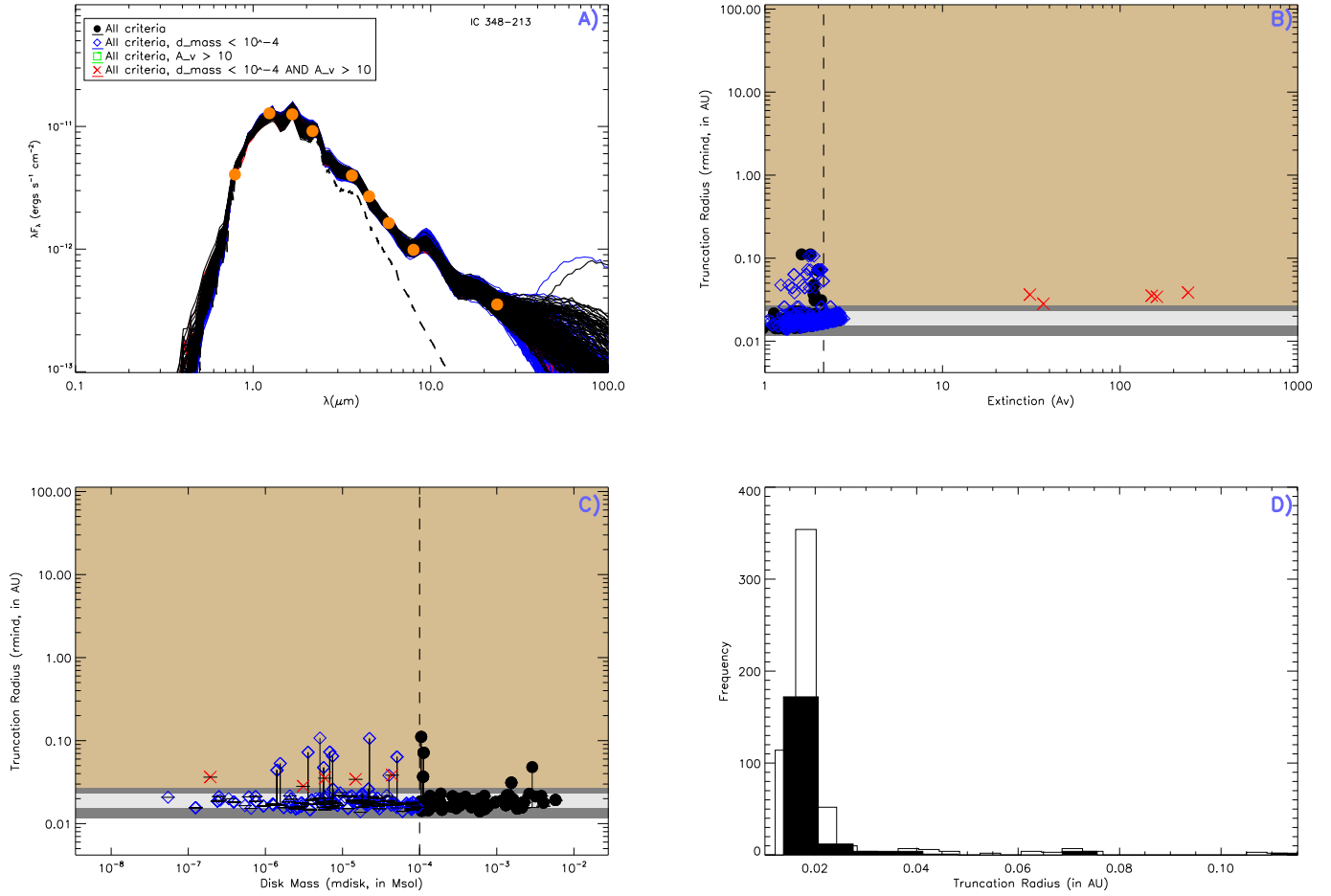


Fig. 31.— IC 348 213. Refer to Figure 2 for further explanation of each of the above panels. Figures 7 - 37 are available in the online version of the Journal.

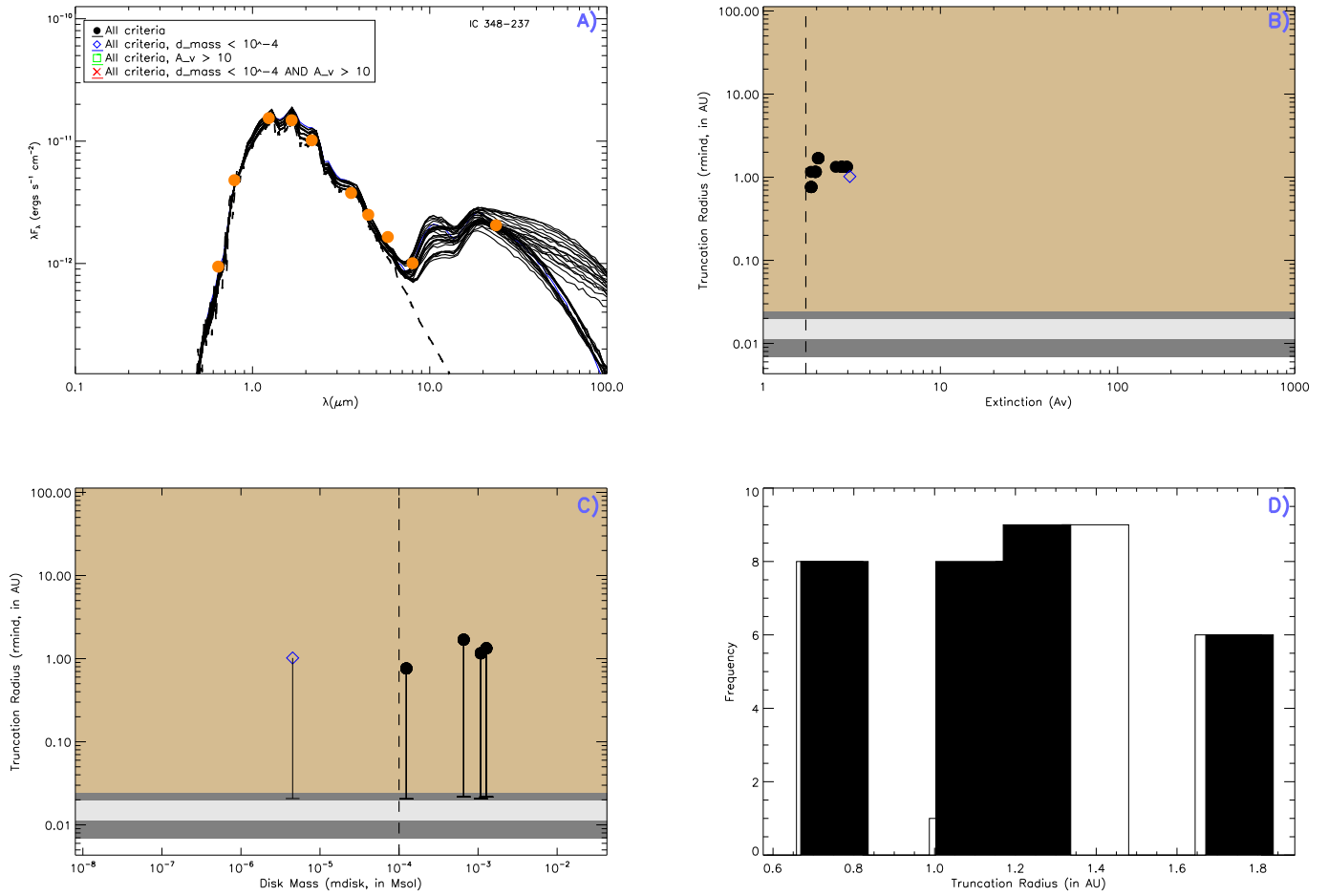


Fig. 32.— IC 348 237. Refer to Figure 2 for further explanation of each of the above panels. Figures 7 - 37 are available in the online version of the Journal.

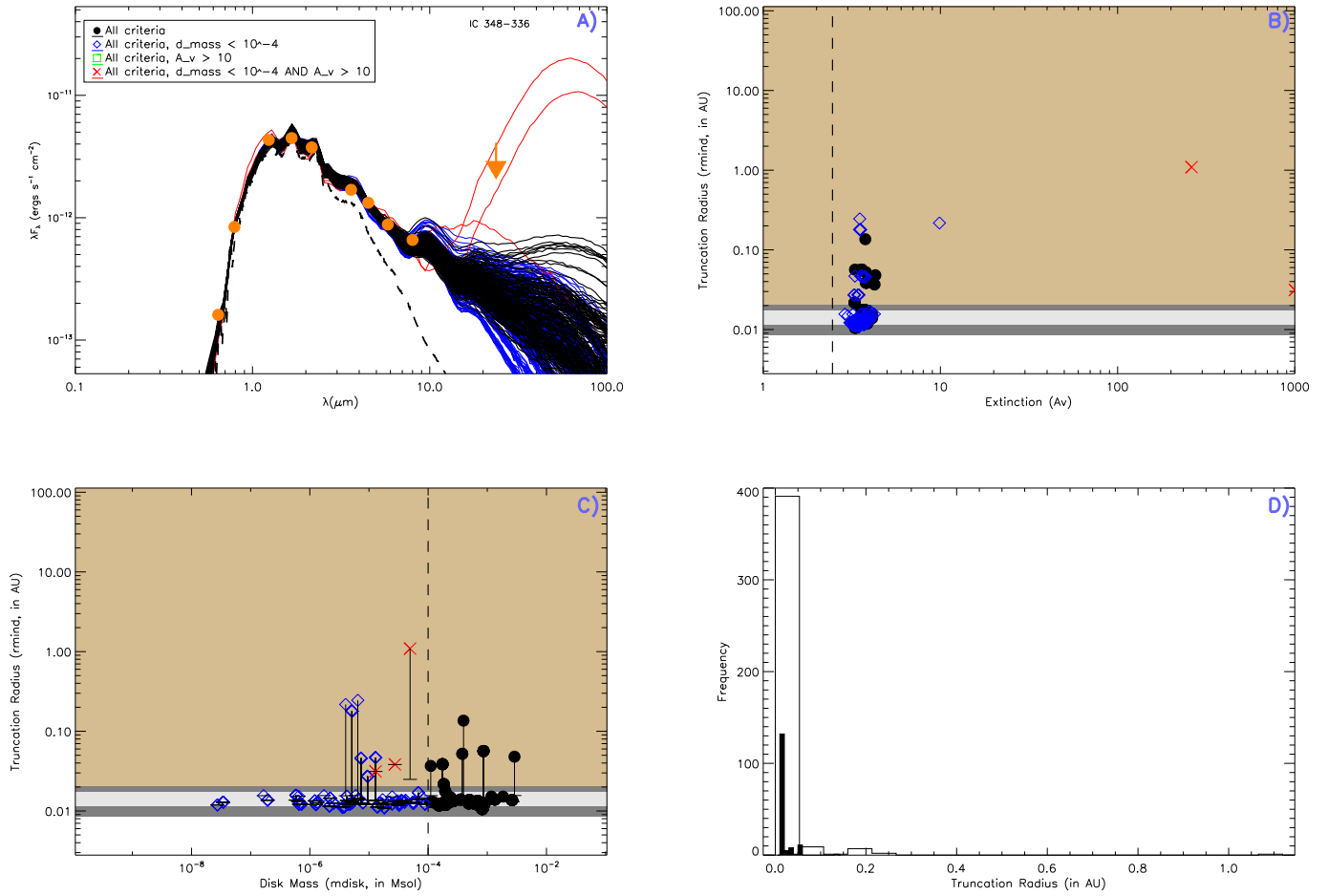


Fig. 33.— IC 348 336. Refer to Figure 2 for further explanation of each of the above panels. Figures 7 - 37 are available in the online version of the Journal.

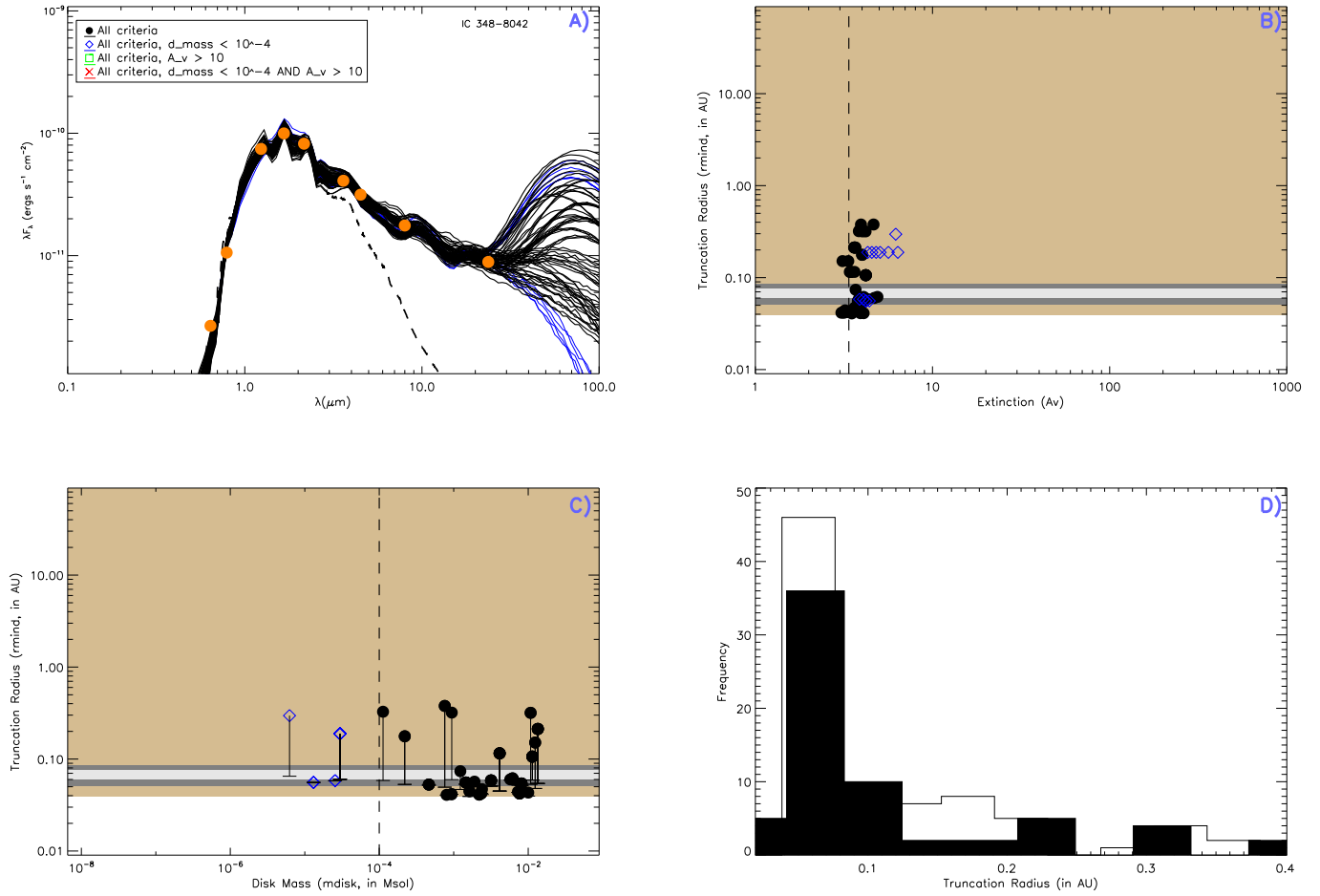


Fig. 34.— IC 348 8042. Refer to Figure 2 for further explanation of each of the above panels. Figures 7 - 37 are available in the online version of the Journal.

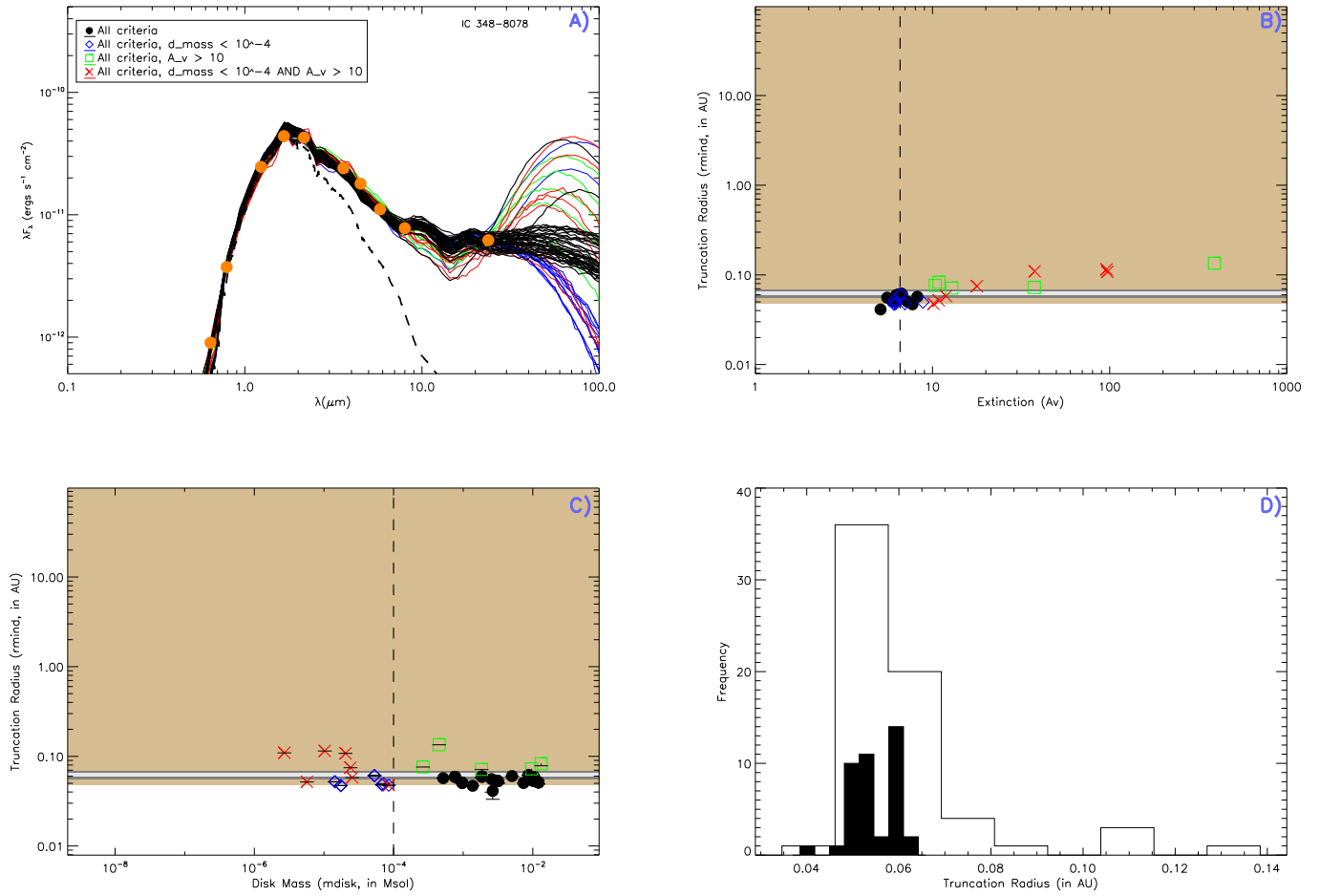


Fig. 35.— IC 348 8078. Refer to Figure 2 for further explanation of each of the above panels. Figures 7 - 37 are available in the online version of the Journal.

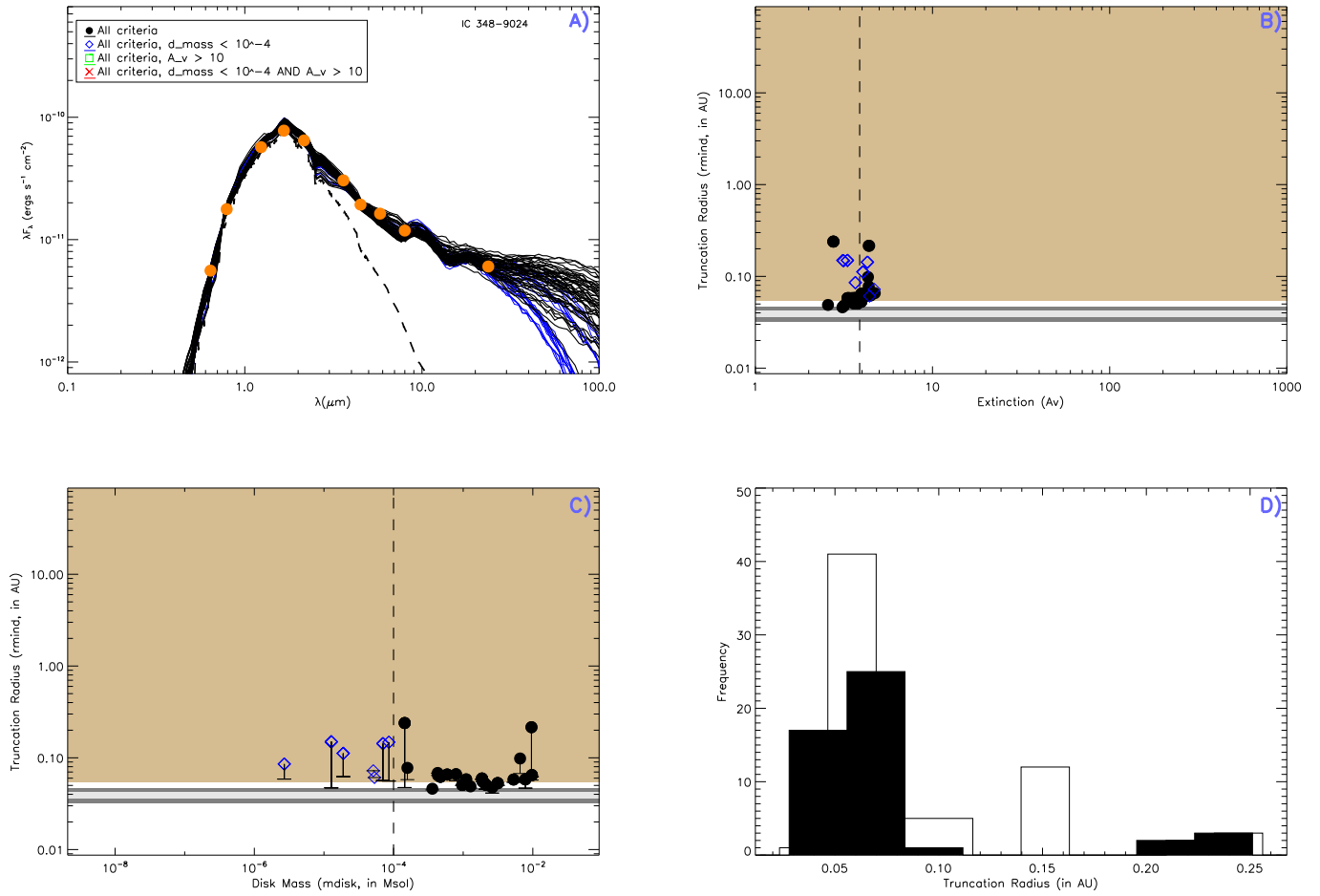


Fig. 36.— IC 348 9024. Refer to Figure 2 for further explanation of each of the above panels. Figures 7 - 37 are available in the online version of the Journal.

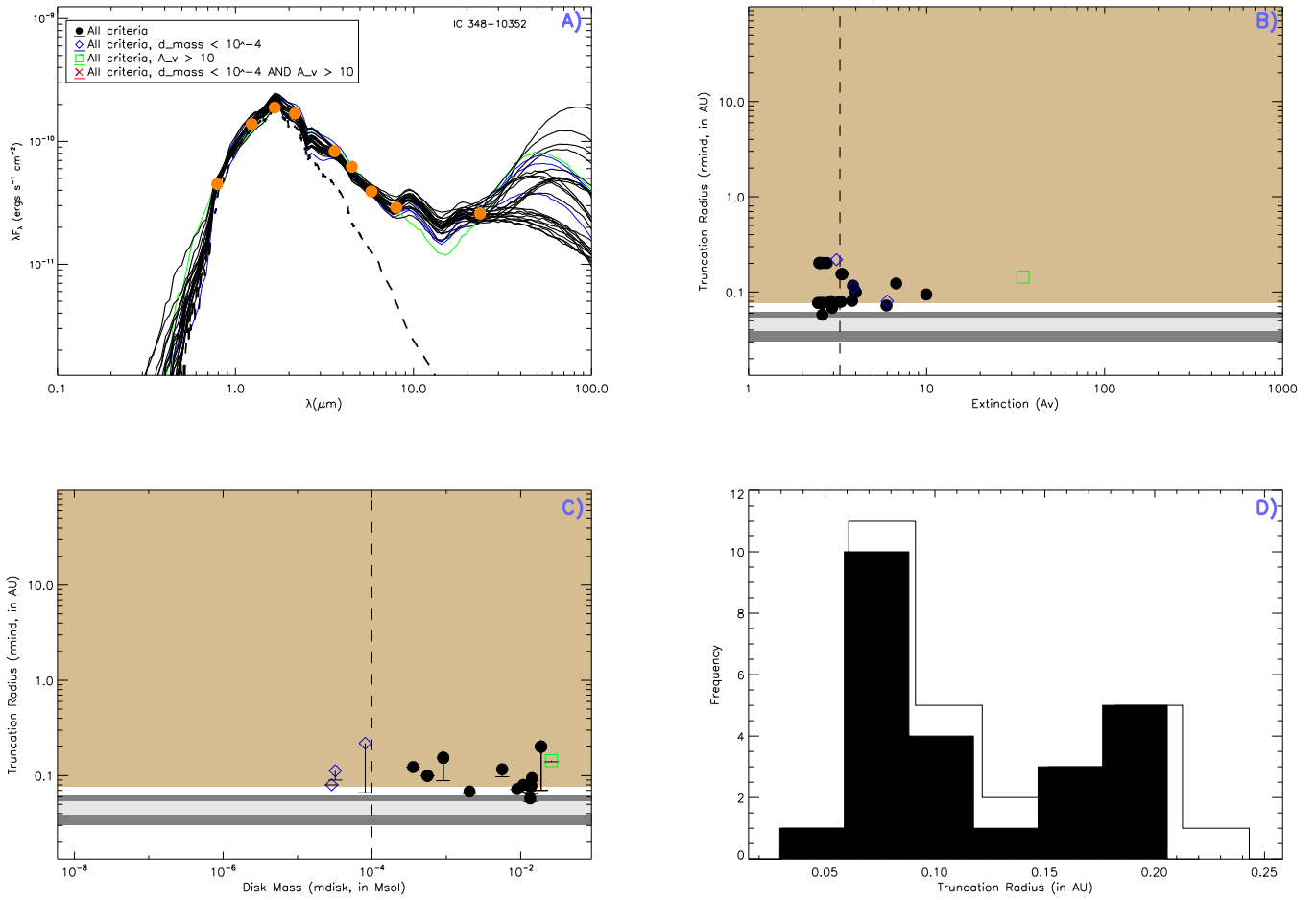


Fig. 37.— IC 348 10352. Refer to Figure 2 for further explanation of each of the above panels. Figures 7 - 37 are available in the online version of the Journal.

Table 1. Photometric Calibration Data

Filter(Type)	$\lambda_{eff}(\mu m)$	Zeropoint (Jy)	Refs.
Johnson[R]	0.64	3072.0	¹
Johnson[I]	0.79	2496.4	¹
2MASS[J]	1.24	1594.0	²
2MASS[H]	1.65	1024.0	²
2MASS[K]	2.17	666.7	²
IRAC[3.6]	3.6	277.3	³
IRAC[4.5]	4.5	179.6	³
IRAC[5.8]	5.8	116.6	³
IRAC[8.0]	8.0	63.1	³
MIPS[24]	24.0	7.14	³

Note. — Calibration data used in converting photometric measurements into flux.

¹Cousins (1976)

²Cohen et al. (2003)

³Fazio et al. (2004)

Table 2. Derived Stellar and Disk Parameters of IC 348 Sample

Star ID	Stellar Parameters from the literature						Disk Radii from SED fitting		
	P_{rot} (d)	T_{eff} (K)	L_{bol} (L_{\odot})	M (M_{\odot}) [†]	R (R_{\odot}) [†]	A_V (mag)	R_{sub} (R_{\star}) [‡]	R_{co} (R_{\star})	R_{trunc} (R_{\star})
32	8.2	4060	1.4	0.48	2.39	5.79	0.08	0.06	0.11
36	5.1	4205	1.5	0.56	2.31	2.91	0.08	0.05	0.51
37	8.6	4205	0.99	0.64	1.87	2.88	0.07	0.07	0.27
58	7.3	3669	0.72	0.31	2.1	2.59	0.06	0.05	0.04
71	6.7	3415	0.47	0.24	1.96	2.14	0.04	0.04	2.66
75	10.6	3669	0.28	0.44	1.31	2.94	0.03	0.07	0.71
76	9.5	3306	0.39	0.19	1.9	2.13	0.04	0.05	0.04
83	8.4	3705	0.51	0.37	1.73	3.43	0.05	0.06	0.04
91	3.9	3560	0.39	0.32	1.64	2.01	0.04	0.03	0.03
97	7.3	3524	0.54	0.28	1.97	4.63	0.05	0.05	1.06
99	7.6	3306	0.26	0.21	1.55	1.91	0.03	0.04	0.04
100	8.4	3705	0.33	0.44	1.39	2.23	0.04	0.06	0.04
110	19.8	3560	0.34	0.34	1.53	4.66	0.04	0.10	2.18
128	2.2	3560	0.32	0.34	1.49	1.73	0.04	0.02	0.03
133	2.1	3125	0.17	0.16	1.41	4.79	0.03	0.02	2.16
149	2.5	3161	0.18	0.17	1.41	3.04	0.03	0.02	0.03
156	1.3	3234	0.17	0.21	1.31	2.04	0.03	0.01	0.02
165	1.9	3091	0.16	0.16	1.39	3.58	0.03	0.02	0.13
166	3.6	3234	0.24	0.18	1.56	5.24	0.03	0.03	0.03
173	2.2	3024	0.12	0.15	1.26	2.57	0.02	0.02	0.02
213	2.3	3161	0.07	0.19	0.9	1.87	0.02	0.02	0.02
237	1.7	3125	0.07	0.18	0.93	2.23	0.02	0.02	1.16
336	1.6	3058	0.03	0.16	0.6	3.6	0.01	0.01	0.01
8042	16	3234	0.37	0.17	1.94	3.97	0.04	0.07	0.06
8078	8.9	3778	0.53	0.42	1.7	6.37	0.05	0.06	0.05
9024	4.5	3850	0.69	0.41	1.87	3.82	0.05	0.04	0.06
10352	6.9	3705	1.4	0.28	2.87	3.7	0.08	0.05	0.10
LB06-100	19.8	3560	0.34	0.34	1.53	4.86	0.04	0.10	0.04

Note. — Derived stellar properties. The radius and mass measurements were derived as described in § 2.2, while temperature, extinction, and luminosity values are from (Luhman et al. 2003), and rotation periods from (Cieza & Baliber 2006). Typical fractional errors for the following parameters are; $T_{eff} \sim 3\%$, $L_{bol} \sim 81\%$, $M_{\odot} \sim 61\%$, and $R_{\odot} \sim 41\%$.

*These extinction values are the original estimates from L03. Our matches in this study for these stars did not yield enough information to make a judgement on the best fit extinction, and are excluded from the final analysis.

[†]Masses and radii were estimated using DM97(?) pre-main sequence evolutionary models (see §2.2), and the Stefan-Boltzmann law, respectively.

[‡]Sublimation radii were estimated using the stellar effective temperature and the sublimation temperature at which the dust in a protoplanetary disk is expected to be destroyed (see §3.1).

Table 3. Discarded IC 348 Sample

Star ID	Stellar Parameters from the literature						Disk Radii from SED fitting		
	P_{rot} (d)	T_{eff} (K)	L_{bol} (L_{\odot})	M (M_{\odot}) [†]	R (R_{\odot}) [†]	A_V (mag)	R_{sub} (R_{\star}) [‡]	R_{co} (R_{\star})	R_{trunc} (R_{\star})
6	1.7	5830	17	2.86	4.04	3.56	0.28	0.04	0.04
21	2.5	5250	3.9	1.48	2.39	5.83	0.13	0.04	0.04
41	2.8	4060	0.79	0.55	1.8	5.76	0.06	0.03	0.03
61	30	3955	0.54	0.55	1.56	4.53	0.05	0.15	0.15
140	12	3379	0.13	0.28	1.05	3.41	0.02	0.07	0.07
182	2.7	3234	0.15	0.2	1.23	3.43	0.03	0.02	0.02

Note. — Derived stellar properties of the discarded sample. Refer to Table 2 for notes.

^{†‡}Refer to Table 2 for notes on masses, radii, and sublimation radii of our sample.